Int J Adv Manuf Technol (2015) 78:361–383
DOI 10.1007/s00170-014-6637-2

ORIGINAL ARTICLE

Numerical investigation of effects of cutting conditions and cooling schemes on tool performance in up milling of Ti-6AL-4V alloy

Jianfeng Ma · Patrick Andrus · Sridhar Condoor · Shuting Lei

Received: 4 June 2014 / Accepted: 23 November 2014 / Published online: 7 December 2014

Abstract Ti-6Al-4V is widely used in industry because of its high strength-to-weight ratio at elevated temperatures, its excellent resistance to fracture and corrosion, and biological properties. However, Ti-6Al-4V is classified as hard-to-cut material because of its high chemical reactivity with most tool materials and its low thermal conductivity that causes high temperature on the tool face. Consequently, prediction of the tool temperature distribution has great significance in predicting tool wear pattern. In this research, finite element method (FEM) is employed to conduct numerical investigation of the effects of cutting conditions (cutting speed, feed rate, and axial depth of cut) in corner up milling on temperature of the tool rake face. The tool material used is general carbide, and the behavior of the workpiece Ti-6Al-4V is described by using Johnson-Cook plastic model. Because of the computational expense, a separate heat transfer model is built to analyze the heat transfer process after the tooth disengages the workpiece and before it engages the workpiece again to predict change of temperature distribution during this cooling process while subjected to different cooling schemes. This research provides helpful guidance for selecting optimal cutting conditions and tool cooling strategies in up milling Ti-6Al-4V alloy.

Keywords Milling · Titanium alloy · FEM simulation · Tool temperature · Heat transfer modeling · Tool cooling

J. Ma (✉) · P. Andrus · S. Condoor
Department of Aerospace and Mechanical Engineering, Saint Louis University, Saint Louis, MO, USA
e-mail: jma15@slu.edu

S. Lei
Department of Industrial and Manufacturing Systems Engineering, Kansas State University, Manhattan, KS, USA

1 Introduction

Ti-6Al-4V is widely used in industry because of its high strength-to-weight ratio at elevated temperatures, its excellent resistance to fracture and corrosion, and biological properties. However, Ti-6Al-4V is classified as hard-to-cut material because of its high chemical reactivity with most tool materials and its low thermal conductivity that causes high temperature on the tool face. This is attributed to their inherently high-strength property maintained at elevated temperatures and their disposition to form localized shear bands during machining. Prediction of tool rake face temperature has great significance in predicting the tool wear pattern since high temperature on tool surface is one of the major leading factors for tool wear. Many researchers have conducted experimental research to investigate how cutting parameters, tool geometries, and initial temperature of the material affect tool temperature distribution in machining Ti-6Al-4V. In the study of Bermingham et al. [1], they investigated the effectiveness of the cryogenic coolant in turning of Ti alloy and found that cryogenic coolant can greatly improve the tool life conditions of high feed rate and low depth of cut combinations. In the study of Liu et al. [2], they experimentally investigated the characteristics of high-speed machining (HSM) dynamic milling forces and found that there exited a characteristic frequency in cutting force power spectrum. In the study of Oosthuizen et al. [3], they investigated the performance of fine-grain polycrystalline diamond (PCD) end mill tool and its wear behavior and found that the PCD tool yielded longer tool life than a coated carbide tool at cutting speeds above 100 m/min and that a slower wear progression with an increase in cutting speeds. In the study of Ghani et al. [4], they experimentally and numerically investigated the tool life and the tool wear behavior of low content CBN cutting tools used in hard turning of hardened H13 tool steel and found that the tool wear was dominated by chipping and could be reduced

considerably by reducing the amount of heat entering the tool. In the study of Alam et al. [5], they investigated the surface roughness in high-speed milling of Ti alloy. In the study of Li et al. [6], they investigated the tool temperature in high-speed milling of Ti-Al6-V4. In the study of Yang et al. [7], they experimentally and numerically investigated the effects of tool edge radius on cutting temperature in micro-end-milling process. Shin and his coworkers experimentally and numerically investigated the tool performance and surface integrity in face milling of Ti-6Al-4V [8]. In the study of Yang et al. [9], they investigated the mechanism of chip formation during high-speed milling of alloy cast iron. In the study of Li et al. [10], they experimentally investigated the effects of the tool material and geometry and drilling process parameters on drill life, thrust force, torque, energy, and burr formation and found that the balance of cutting speed and feed is essential to achieve long drill life and good hole surface roughness. Li et al. conducted metallurgical analysis and nanoindentation characterization of Ti-6Al-4V workpiece and chips in high-throughput drilling to investigate the influence of high temperature, large strain, and high strain rate deformation on phase transformation and mechanical properties [11].

In addition to experimental research to investigate the tool temperature in machining Ti-6Al-4V, many researchers have been conducting numerical simulations of Ti-6Al-4V machining to improve its machinability [12–17] using finite element method (FEM). Li and Shih conducted finite element modeling of 3D turning of titanium to investigate the effects of cutting speed, the depth of cut, and the tool cutting edge radius on the peak tool temperature [12]. In the study of Wang et al. [13], they modeled the cutting forces of machining of Ti alloy with different coolant strategies. Huang and Yao simulated HSM temperature of Ti alloy [14]. In the study of Soo [15], Soo used 3D FEM to investigate the high-speed ball nose end milling. In the study of Saffar et al. [16], they conducted 3D FEM modeling of cutting force and tool deflection in the end milling operation. In the study of Ali et al. [17], they used FEM to predict the effects of feed rate on surface roughness with cutting force during face milling of titanium alloy. Numerical simulation of turning of Ti alloys to predict chip formation process and cutting forces has been the main focus. In addition, most of the milling simulations on Ti-6Al-4V have been focusing on end-milling. Numerical simulation of intermittent milling processes, especially corner milling and face milling, has not been widely conducted. Most of the numerical simulations that have been conducted focused on the cutting period of the milling process and not on the nonmilling period when the insert is being cooled by the surrounding air [18, 19]. In the study of Wu and Mayer [18], they used FEM to investigate the transient temperature and thermal stress distribution in carbide tool during intermittent cutting. In the study of Chakraverti et al. [19], they used an analytical model to predict tool temperature fluctuation in interrupted cutting. In this research, 3D numerical simulation is conducted to investigate the effects of the milling parameters (cutting speed, feed rate, and axial depth of cut) in up corner milling on tool rake face temperature using AdvantEdge FEM [20]. After the FEM simulations are conducted, heat transfer FEM simulations are performed using Abaqus to investigate the temperature change of the insert that would occur during the time period when the insert does not engage in cutting the workpiece (noncutting period) and is in contact with the surrounding air and other coolants. FEM simulations give the capability of accessing data that is nearly physically impossible, such as the temperature, stresses, and other variables at the tool-chip interface. Prediction of the tool temperature benefits the optimization of the cutting conditions and assists designing better tooling and cooling schemes in order to improve the Ti alloys' machinability. Due to the low thermal conductivity of Ti alloys, which is an inherent property of this group of materials, it is highly desirable that the temperature of tool insert can be lowered to room temperature after tool insert disengages the workpiece in order to avoid the accumulation of the heat along tool-chip contact length when the tool insert engages the workpiece again. The aim of this research is to investigate the effects of cutting conditions on tool temperature, the effects of different cooling schemes during the noncutting period of the milling process to lower the temperature of the tool insert before the tool insert reengages the workpiece. In addition, the effects of the cutting conditions and cooling schemes on the tool insert thermal stress are also investigated. This research provides insights of cutting conditions and cooling schemes under which tool life can be increased.

2 3D FEM simulation

The setup of 3D FEM corner milling model is presented in Fig. 1. The setup of the FEM simulation is a single insert cutter, up milling, cornering simulation. Figure 2 shows 3D FEM modeling of corner milling with temperature distribution at one instant. The height, width, and length of the workpiece are 5, 10, and 24 mm, respectively.

The model utilizes the updated Lagrangian finite element formulation in conjunction with continuous meshing and adaptive meshing techniques. The bottom surface of workpiece is fixed in z direction, and the tool rotates about the *z*-axis. The convergence tests have been conducted in order to obtain the reliable numerical results. The maximum element size of the workpiece is set as 2 mm, and the minimum element size is set as 0.0198 mm. The maximum element size of the tool cutter edge is set as 0.3 mm, and the minimum element size is set as 0.01 mm. The radius of the refined region on the cutter's edge is set to 0.075 mm. A mesh refinement factor of five is used, and the mesh coursing factor of five is

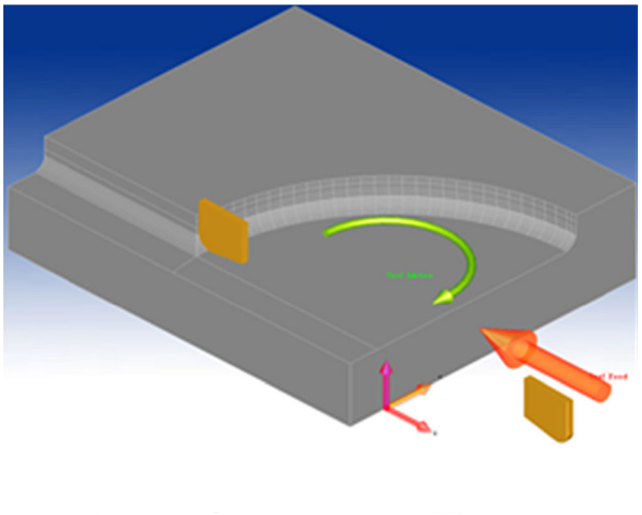

Fig. 1 The setup of 3D FEM corner milling

utilized. The tool boundary conditions are specified such that the top surface of the tool is fixed in vertical direction. The workpiece is constrained in both lateral and vertical directions on its bottom surface. The relative motion between the tool and the workpiece is realized by the rotation of the tool at specified cutting speeds. Adiabatic thermal boundary condition is applied on all the faces of tool except the one that interacts with the workpiece. Tables 1 and 2 give the tool geometry and cutting conditions, respectively.

Table 1 Tool geometry

Tool dimensions	
Cutter diameter (mm)	101.6
Width of tool (mm)	0.3
Lead angle (deg)	30
Radial rake angle (deg)	2
Axial rake angle (deg)	5
Relief angle (deg)	11
Edge radius (mm)	0.02
Nose radius (mm)	0.4

Ti-6Al-4V material properties

FEM simulations are accurate and reliable only when the correct properties are entered. AdvantEdge has a database of already prescribed material properties for both tools and workpieces. In the case of Ti-6Al-4V, the default material properties have proven not to produce accurate results [21]. Therefore, user-defined material properties for titanium need to be used. Material properties of Ti-6Al-4V and tool material carbide are given in Table 3. In this research, the Johnson-Cook model is employed to describe the material behavior of the titanium alloy (Ti-6Al-4V). This is due to its capability of the model to accurately determine strain, strain rate, and temperature dependency. The model is expressed as Eq. (1). Where σ is the equivalent stress, ε is the plastic strain, $\dot{\varepsilon}$ is the strain rate, $\dot{\varepsilon}_0$ is the reference strain rate, T is the operating temperature, T_r is the room temperature, T_m is the melting temperature, A is the initial yield stress, b is the hardening modulus, n is the work hardening exponent, C is the strain rate-dependent coefficient, and m is the thermal softening coefficient. The variables for the Johnson-Cook model are given in Table 4.

$$\sigma = \left(A + B\varepsilon_p^n\right)\left(1 + C\,\mathrm{In}\left(\frac{\dot{\varepsilon}}{\dot{\varepsilon}_0}\right)\right)\left(1-\left(\frac{T-Tr}{Tm-Tr}\right)^m\right) \quad (1)$$

The thermal properties of the material, thermal conductivity, and specific heat are also included in the model. The properties for Ti-6Al-4V from the study of Mills [23] have shown to give good results in the study of Rao et al. [8]. Equations 2 and 3 are used to calculate the thermal conductivity (k, W/m°C), and Eqs. 4 and 5 are used to calculate the

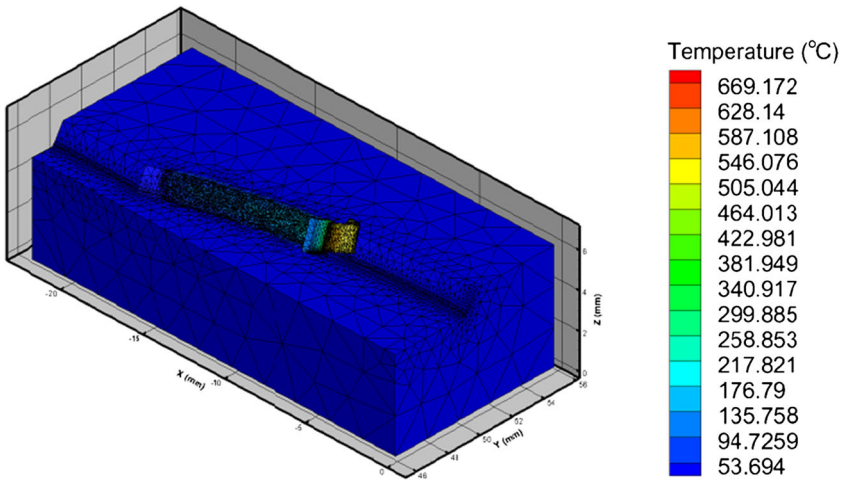

Fig. 2 3D FEM corner milling simulation

Table 2 Cutting conditions

Corner, up milling cutting parameters	
Cutting speed (m/s)	0.5, 1, 2
Feed rate (mm/tooth)	0.1, 0.2, 0.4
Radial width of Cut (mm)	3
Axial depth of cut (mm)	0.5, 1 , 1.5
Initial temperature (°C)	20
Friction coefficient	0.65

Table 4 Johnson-Cook material model for Ti-6Al-4V

Johnson-Cook model parameters	
A (MPa)	1080
B (MPa)	1007
C	0.01304
n	0.6349
m	0.77
$\dot{\varepsilon}_0$	1.0

specific heat (C_p, J/kg°C). In AdvantEdge FEM, a table of 50 entries is defined for the temperature-dependent thermal conductivity and specific heat. For the Eqs. 2 and 4, 25 entries are calculated until the temperature reaches 986.85 °C. For the Eqs. 3 and 5, 25 entries are calculated until the temperature reaches the melting point of Ti-6Al-4V.

$$T \leq 986.85^{\circ}\mathrm{C},\ k = 1{*}10^{-5}T^2 - 0.00112T + 6.651 \quad (2)$$

$$T > 986.85^{\circ}\mathrm{C},\ k = -4{*}10^{-6}T^2 + 0.0253T - 6.269 \quad (3)$$

$$T \leq 986.85^{\circ}\mathrm{C},\ C_p = .21T + 483.3 \quad (4)$$

$$T > 986.85^{\circ}\mathrm{C},\ C_p = .18T + 420.19 \quad (5)$$

3 Validation of 3D corner milling FEM model

The 3D corner milling model is validated by comparing numerical results with experiments given in the study of Rao et al. [8]. Table 5 shows the comparison of numerical results with the experimental results obtained in the study of Rao et al. [8] in terms of specific cutting energy, temperature, and von Mises stress in the primary deformation zone, temperature, and the von Mises stress in the secondary deformation zone, and tool chip contact length. For the simulation used here, the cutting conditions are the following: 1.27 m/s cutting speed; 0.0508 mm feed rate; 0.762 mm depth of cut. The tool geometry is the following: 0.024 mm edge radius; 0.8 mm nose radius; 5° axial rake angle; and 2° radial rake angle. The above cutting conditions and tool geometry are very close to the cutting conditions and tool geometry used in this research. It is clear that the numerical results fall in between the ranges used in the study of Rao et al. [8], and it can be said that FEM model can be used to simulate corner milling with adequate accuracy.

Table 3 Material properties of Ti-6Al-4V and tool material carbide [22]

Material properties	Ti-6Al-4V	Carbide
Elastic modulus (GPa)	114	705
Density (kg/m^3)	4428	15290
Poisson's ratio	0.34	0.23
Coefficient of thermal expansion (1/°C)	9.6×10^{-6}	7.1×10^{-6}
Melting temperature (°C)	1659.85	2800
Room temperature (°C)	22.85	22.85

4 Abaqus free convection to air heat transfer FEM model

Because of the computational expense associated with continuous simulation for inserts and the lack of the capability of AdvantEdge FEM to predict the tool temperature distribution before each of the inserts reengages workpiece again, a heat transfer FEM model is created using general purpose FEM commercial software Abaqus [24].

The initial temperature distribution of the insert is obtained by importing the final tool temperature distribution from AdvantEdge FEM into Abaqus. Figure 3 shows the final temperature distribution of one of the AdvantEdge simulations. Figure 4 shows the initial temperature distribution of one of the Abaqus simulations. To import the insert temperature data from AdvantEdge FEM model into the Abaqus model, a python code is developed which uses a 3D rotation matrix to position the data obtained from AdvantEdge FEM into the correct orientation in Abaqus. Due to the change in programs and orientation, a comparison between the temperature distribution obtained from AdvantEdge FEM and the temperature distribution of the Abaqus model is conducted. The comparison shows that the maximum error between temperature values from AdvantEdge FEM and Abaqus is 3.17 %, which means that the python code can import the temperature from AdvantEdge to Abaqus within very high accuracy. Consequently, Abaqus model can be used to conduct heat transfer simulation to predict the tool temperature

Table 5 Comparison between simulation results and experimental results

Rao et al. (2011) [8]		Simulation	
Primary cutting zone	Range	Primary cutting zone	Average
Temperature (°C)	475–580	Temperature (°C)	541.24
von Mises Stress (Mpa)	1180–1390	von Mises Stress (Mpa)	1260.04
Secondary cutting zone		Secondary cutting zone	Average
Temperature (°C)	580–750	Temperature (°C)	591.49
von Mises Stress (Mpa)	180–370	von Mises Stress (Mpa)	220.14
Specific cutting energy x10^6 (J/m^3)	2300–2800	Specific cutting energy x10^6 (J/m^3)	2756.75
Tool-chip contact length (mm)	0.1	Tool-chip contact length (mm)	0.122

changes from the instant the tool insert disengages the workpiece to the instant it reengages the workpiece again.

The boundary conditions for the insert are free convection to the air on all sides except for the adjacent edges to the leading edge where it is simplified to be adiabatic. In actuality at these locations, the insert material would continue to form the entire insert. The 4-node linear heat transfer tetrahedron elements (DC3D4) are used in Abaqus heat transfer model. The simulation parameters can be found in Table 6. In Table 6, the film coefficient is for free convection to air, and the parameter of time is the length of time for the insert to reengage the workpiece for the different three cutting speeds tested in AdvantEdge.

The meshing of the model in Abaqus is set as biased seeding, multiple seeding, with the leading edge having a very fine mesh and the rest of the part having a coarser mesh. The leading edges have an element size of 0.025 mm, and the rest of the model has an element size of 0.074 mm. This meshing setup results in an element count of 97,514. The mesh for the part can be seen in Fig. 5.

A convergence test is performed for the Abaqus heat transfer simulation for both effects of the mesh to the initial temperature distribution and performance of the simulation with the time parameter of 0.30411 s (which corresponds to the cutting speed of 1 m/s), the depth of cut of 1.5 mm, and feed rate of 0.2 mm/tooth. In the convergence test for the initial temperature, 3 mesh counts are tested by taking the temperature values of 20 nodes in Abaqus and comparing the values to the same location in AdvantEdge. The results of the test showed that the % errors are all below 5 %. These results show that the element count has little effect on the initial temperature distribution. The range of % error can be found in Table 7.

In the convergence test for the performance of the simulation, six different meshes are tested to find the optimal simulation, a balance of low computer computation, and high accuracy. This is found by taking the value of a specified point in all of the simulations and comparing the difference between the previous simulation and the current one. As the difference reduces, the reliability of the simulation increases. For the heat transfer, tests are performed by taking the corner node with the highest temperature in Abaqus. The same node is used in all simulations to compare the temperature at the end. The simulation parameters used to this test is the following: the time parameter of 0.30411 s (cutting speed of 1 m/s), the depth of cut of 1.5 mm, and feed rate of 0.2 mm/tooth. Figure 6 shows the variation of the temperature as the mesh count increases, and Fig. 7 shows the % error between two

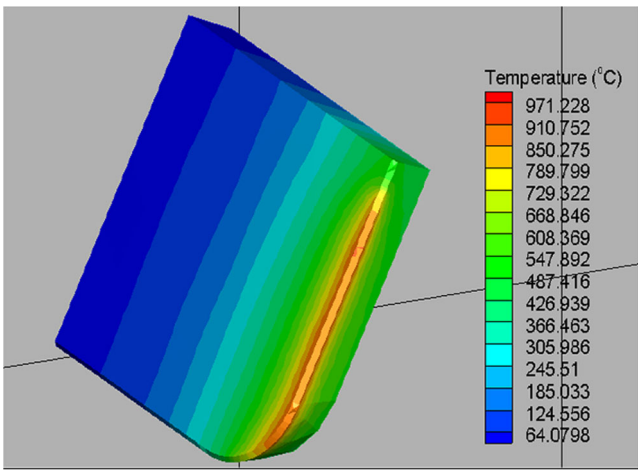

Fig. 3 3D AdvantEdge FEM model

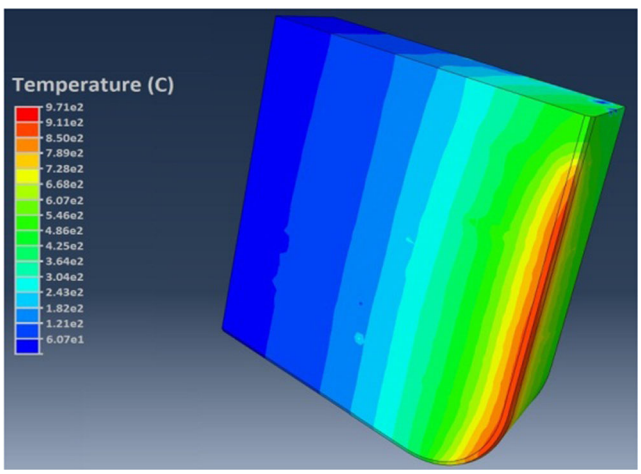

Fig. 4 3D heat transfer Abaqus model

Table 6 Tool insert heat transfer parameters

Heat transfer parameters	
Time (seconds)	0.60828, 0.30411, 0.15207
Film coefficient (W/m^2 °C)	17.04
Room temperature (°C)	22.85

neighboring meshes. The results show that the optimal mesh count is 97,514 and node count is 18,782, element sizes are given above, with a % error of 0.0843 %.

There are many factors that can affect the exact film coefficient; therefore, a sensitivity test is conducted to determine the effect of the film coefficient to the simulation using values in the accepted range from 5 to 20 W/m^2 °C for free convection to air. The simulation tested here is using the time period 0.30411 s (cutting speed of 1 m/s), the depth of cut of 1.5 mm, feed rate of 0.2 mm/tooth, and the optimal mesh of 97,514 elements. The results in Fig. 8 show that there is only a 4.33 °C difference between the lowest and highest values in the range. This shows that for the Abaqus heat transfer simulation, the film coefficient has little effect in this range. The film coefficient use in this research is 17.04 W/m^2 °C, which can be found in previous literature for free convection [25].

5 Abaqus convection to coolant heat transfer FEM model

In continuation of studying the effects of cooling the tool insert after it has disengaged the workpiece, different coolants are applied to the insert during this stage. It should be noted that no coolant is applied during the milling process and coolants are applied only during noncutting period. These tests are conducted using the previous initial temperature distribution, parameter of time, and boundary conditions on the insert. The only difference in the simulations is the values for the boundary conditions for the insert, which are the convection to the coolant being used in the simulation. Table 8 shows the parameters of the coolants used in Abaqus. These parameters have been used in previous literature for convection to the coolants [8, 26].

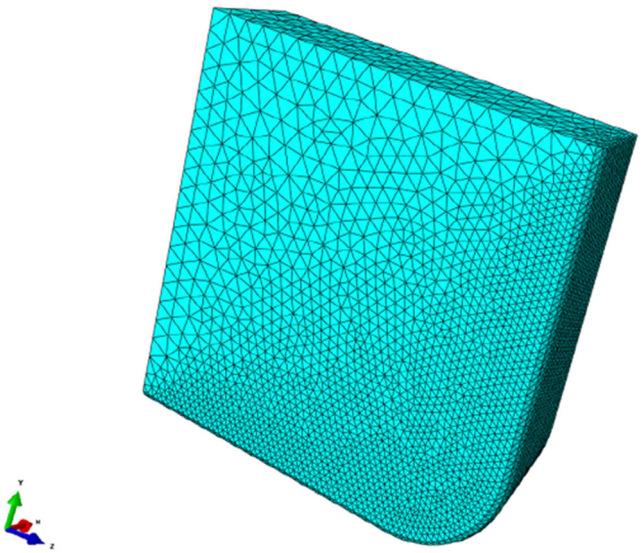

Fig. 5 Mesh for the tool insert

Table 7 Initial convergence test

Element; node count	Range of % error
1122; 328	0.02–2.49
97514; 18782	0.24–3.17
526373; 96647	0.04–2.8

Sensitivity tests for these coolants are conducted due to the fact that film coefficients for different simulations are different due to the differences of the inserts used and the way the coolant is applied. The simulation used to test the sensitivity of the coolants is the time period 0.30411 s (cutting speed of 1 m/s), the depth of cut of 1.5 mm, feed rate of 0.2 mm/tooth, and the optimal mesh of 97,514 elements.

For the TrimSol 5 % concentrate water-based coolant (flood), a film coefficient range of 4500–6000 W/m^2 °C is tested, and the results, seen in Fig. 9, show us that in this range, the difference in the final temperatures is a 4.68 °C between the lowest and highest values in the range. Thus, the effect of the change in film coefficient is small. The film coefficient use in this research is 5230 W/m^2 °C, which is obtained in the study of Kurgin [26].

In the sensitivity test for the heavy duty water-soluble oil-based cutting fluid, a range of 500–2500 W/m^2 °C is tested, and the results, seen in Fig. 10, show us that in this range, the difference in the final temperatures is a 173.01 °C between the lowest and highest values in the range. Thus, the effect of the change in film coefficient could have an effect on the study; however, since the range of the test is large, the reliability of the value used is still valid. The film coefficient used in this research is 1500 W/m^2 °C, which is obtained from the study of Rao [8].

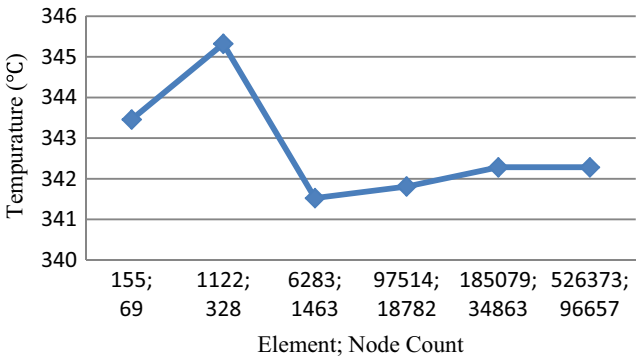

Fig. 6 Temperature values tested in second convergence test

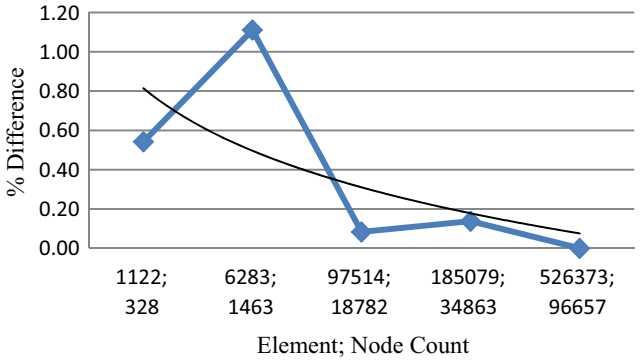

Fig. 7 % difference of the temperature values tested in second convergence test

In the sensitivity test for the emulsion coolant, a range of 80,000–95,000 W/m^2 °C is tested, and the results, seen in Fig. 11, show us that in this range, the difference in the final temperatures is a 0 °C between the lowest and highest values in the range. Thus, the effect of the change in film coefficient has little to no effect. The film coefficient use in this research is 87,500 W/m^2 °C, which is obtained from the study of Rao [8].

In the sensitivity test for the liquid nitrogen, a range of 20,000–50,000 W/m^2 °C is tested, and the results, seen in Fig. 12, show us that in this range, the difference in the final temperatures is almost 0 °C (0.006 °C) between the lowest and highest values in the range. Thus, the effect of the change in film coefficient has little to no effect. The film coefficient use in this research is 35,000 W/m^2 °C, which is in-between the range of values that is calculated in previous literature (23,270–46,750 W/m^2 °C) [8].

6 Thermal stress calculations

The change of temperature in materials causes them to expand when heated and contract when cooled. This process can cause damage to the material in the form of thermal stress and possibly cracking of the material. This is the case for milling processes due to the fact that there is a cutting portion, which causes heating, and then a noncutting portion, causing cooling. Over time, thermal stress can lead to possible tool failure [18, 27–29]. Equation 6 calculates the thermal stress, where σ_t is the thermal stress, α is the coefficient of thermal expansion, E is the elastic modulus, and Δt is the change in temperature.

$$\sigma_t = \alpha * E * \Delta t \tag{6}$$

Table 8 Coolant heat transfer parameters

Coolant	Temperature (°C)	Film coefficient (W/m^2 °C)
TrimSol 5 % concentrate water-based coolant (flood)	20	5230
Heavy duty water-soluble oil based cutting fluid	20	1500
Emulsion coolant	25	87500
Liquid nitrogen	−196	35000

7 Numerical results

This section presents the numerical results of the heat transfer of carbide inserts to surrounding air, TrimSol 5 % concentrate water-based coolant, heavy duty water-soluble oil-based cutting fluid, emulsion coolant, and liquid nitrogen using Abaqus. The effects of cutting speed, feed rate/tooth, and axial depth of cut on the final temperature distribution are analyzed and discussed.

In this section, the temperature history is for the point that has the highest initial temperature because the initial temperature distribution is not uniform for each of these simulations. It should be noted that the point that has the highest initial temperature is located on the cutting edge for each of this

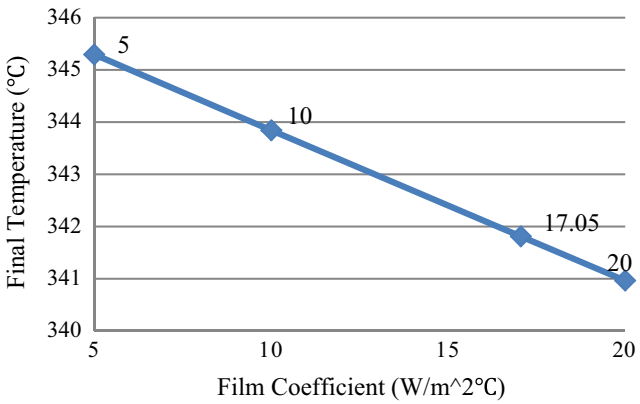

Fig. 8 Sensitivity test of the film coefficient for free convection to air

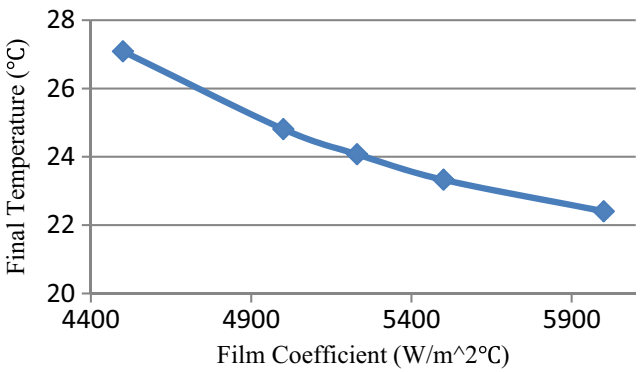

Fig. 9 Sensitivity test of the film coefficient for convection to TrimSol 5 % concentrate water-based coolant

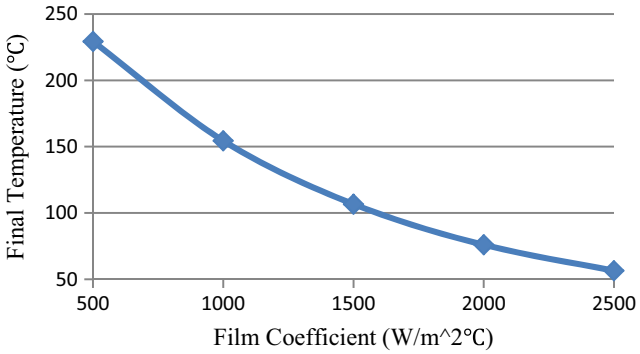

Fig. 10 Sensitivity test of the film coefficient for convection to heavy duty water-soluble oil-based cutting fluid

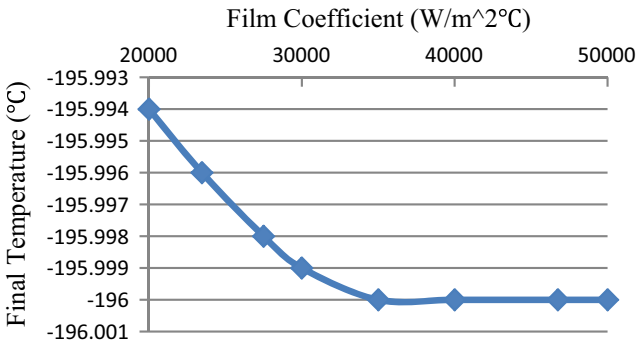

Fig. 12 Sensitivity test of the film coefficient for convection to liquid nitrogen

simulation. However, the exact location of this point is different for different simulations.

In addition, it should be noted that in the following sections, the initial tool temperature distribution refers to the tool temperature distribution immediately after the tool disengages the workpiece, which means that the tool temperature distribution is at the end of milling simulation. The final tool temperature distribution refers to the tool temperature distribution immediately before the tool reengages the workpiece after certain amount of time of the cooling in the coolant.

7.1 The effect of cutting speed/duration of time for noncutting periods

In these simulations, three speed values (0.5, 1, and 2 m/s) are used in this research by converting to duration of time for noncutting periods (0.60828, 0.30411, and 0.15207 s, respectively). For all these three simulations, the feed rate is 0.2 mm/tooth, and axial depth of cut is 1 mm. The film coefficients (17.04, 5230, 1500, 87,500, and 3500 W/m^2 °C) and coolant initial temperatures (22.85, 20, 20, 25, and −196 °C) are changed, respectively (air, TrimSol 5 % concentrate water-based coolant, heavy duty water-soluble oil-based cutting fluid, emulsion coolant, and liquid nitrogen). It should be noted that for different coolants, the initial tool temperature distribution is the same for the same cutting conditions. The initial maximum temperature for 0.5, 1, and 2 m/s cutting speed is 678, 772, and 893 °C, respectively. Therefore, the initial temperature distribution for the same cutting condition is only presented once, as shown in this subsection.

7.1.1 The effect of cutting speed/duration of time for noncutting periods subjected to surrounding air

Figure 13 shows the temperature history for these three simulations. The final temperature for 0.5, 1, and 2 m/s cutting speed is 323 °C, 260 °C, and 203 °C, respectively. In addition, it should be noted that for all three cutting speeds, the final temperature distribution is uniform. Figure 14 is a simplification of the temperature history only using the initial temperature and final temperature. It is clearly seen that the highest cutting speed has the highest initial maximum temperature and the lowest final temperature while the lowest cutting speed has the lowest initial temperature and the highest final temperature.

In Fig. 15a, the left plot shows the initial temperature distributions, and the right plot shows the internal horizontal segment cut out of the temperature distribution half way through for cutting speed 0.5 m/s. In Fig. 15b, the left plot shows the initial temperature distributions, and the right plot shows the internal horizontal segment cut out of the temperature distribution half way through for cutting speed 1 m/s. In

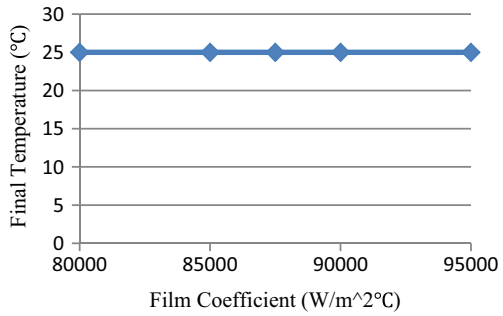

Fig. 11 Sensitivity test of the film coefficient for convection to emulsion coolant

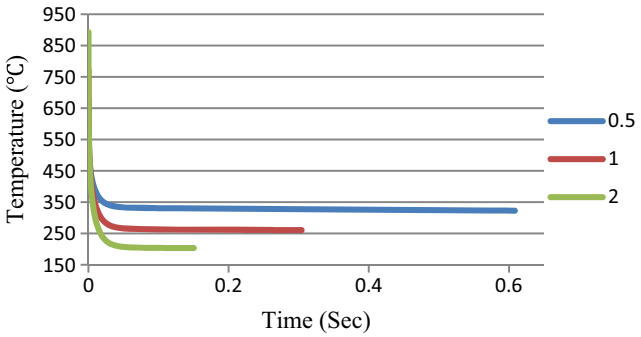

Fig. 13 Temperature history for three different cutting speeds for surrounding air

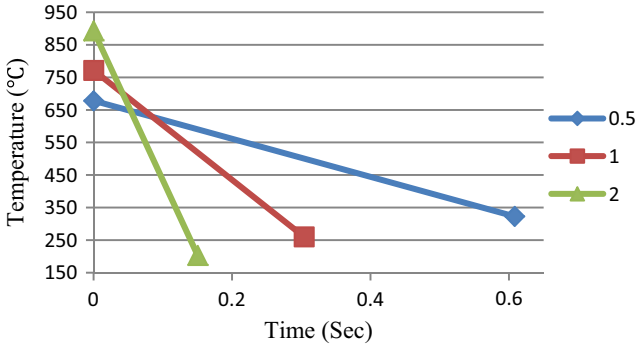

Fig. 14 Simplified temperature history for three different cutting speeds using only the initial and final temperatures for surrounding air

Fig. 15c, the left plot shows the initial temperature distributions, and the left plot shows the internal horizontal segment cut out of the temperature distribution half way through for cutting speed 2 m/s. It is noted that the lowest cutting speed has the lowest temperature distribution along the rake face but highest internally while the highest cutting speed has the highest temperature distribution along the rake face but lowest internally. This helps to explain why the highest cutting speed (2 m/s) has the highest initial temperature on the rake face but has the lowest uniform final temperature. It should be noted that in Fig. 15, all plots use the same legend scale so that there is no red zone in Fig. 15a because the red zone is for temperatures that are greater than 819 °C. The horizontal segment cut out in the right plot of 15a, 15b, and 15c starts at point 1 and continues to point 2.

7.1.2 The effect of cutting speed/duration of time for noncutting periods subjected to TrimSol 5 % concentrate water-based coolant

Figure 16 shows the temperature history for these three simulations. The final temperature for 0.5, 1, and 2 m/s cutting speed is 20 °C, 23 °C, and 39 °C, respectively. Figure 17 is a simplification of the temperature history only using the initial temperature and final temperature. It is manifest that the highest cutting speed has the highest initial temperature and the highest final temperature while the lowest cutting speed has the lowest initial temperature and the lowest final temperature. It should be noted that for all of these three simulations, the final temperature distribution is uniform.

7.1.3 The effect of cutting speed/duration of time for noncutting periods subjected to heavy duty water-soluble oil-based cutting fluid

Figure 18 shows the temperature history for these three simulations. The final temperature for 0.5, 1, and 2 m/s cutting speed is 43 °C, 85 °C, and 115 °C, respectively. Figure 19 is a simplification of the temperature history only using the initial temperature and final temperature. It is noted that the highest cutting speed has the highest initial temperature and the highest final temperature while the lowest cutting speed has the lowest initial temperature and the lowest final temperature. For all of these three simulations, the final temperature distribution is uniform.

7.1.4 The effect of cutting speed/duration of time for noncutting periods subjected to emulsion coolant

Figure 20 shows the temperature history for these three simulations. The final temperature for 0.5, 1, and 2 m/s cutting speed is 25 °C, 25 °C, and 25 °C, respectively. Figure 21 is a simplification of the temperature history only using the initial temperature and final temperature. It is concluded that the highest cutting speed has the highest initial temperature and the lowest cutting speed has the lowest initial temperature with

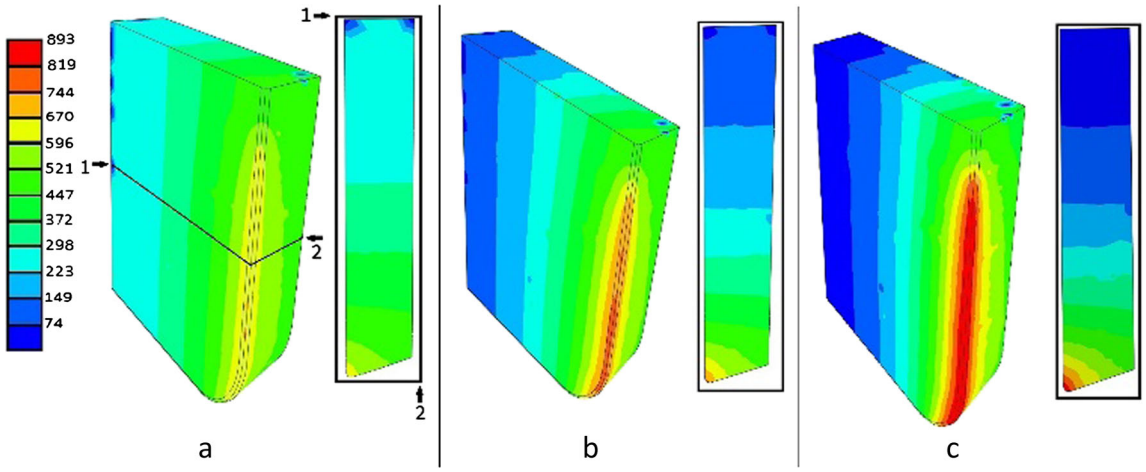

Fig. 15 Initial temperature distributions and internal horizontal segment cut out of the temperature distribution half way through for three different cutting speeds (0.5, 1, and 2 m/s, respectively)

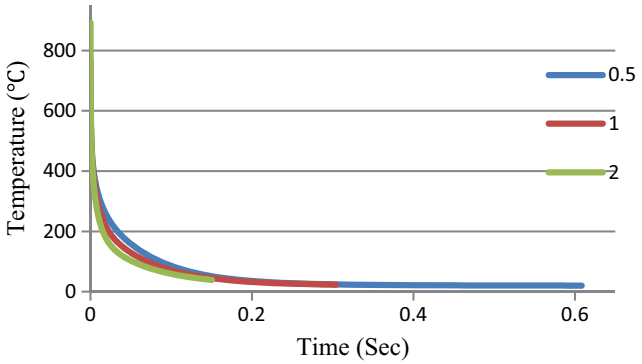

Fig. 16 Temperature history for three different cutting speeds for TrimSol 5 % concentrate water-based coolant

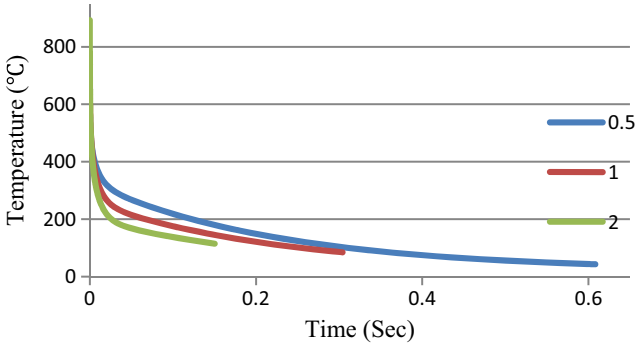

Fig. 18 Temperature history for three different cutting speeds for heavy duty water-soluble oil-based cutting fluid

all of the cutting speeds having the same final temperature, the temperature of the coolant.

It should be noted that for all of these three simulations, the final temperature distribution is uniform.

7.1.5 The effect of cutting speed/duration of time for noncutting periods subjected to liquid nitrogen

Figure 22 shows the temperature history for these three simulations. The final temperature for 0.5, 1, and 2 m/s cutting speed is −196 °C, −196 °C, and −196 °C, respectively. Figure 23 is a simplification of the temperature history only using the initial temperature and final temperature. It is manifest that the highest cutting speed has the highest initial temperature and the lowest cutting speed has the lowest initial temperature with all of the cutting speeds having the same final temperature, the temperature of the coolant. It should be noted that for all of these three simulations, the final temperature distribution is uniform.

7.2 The effect of depth of cut for noncutting periods

In these simulations, three depth of cut values (0.5, 1, and 1.5 mm) are used in this research. For all these simulations, the feed rate is 0.2 mm/tooth and axial depth of cut is 1 mm. The film coefficients (17.04, 5230, 1500, 87,500, and 3500 W/m^2 °C) and coolant temperatures (22.85, 20, 20, 25, and −196 °C) are changed, respectively (air, TrimSol 5 % concentrate water-based coolant, heavy duty water-soluble oil-based cutting fluid, emulsion coolant, and liquid nitrogen). It should be noted that for different coolants, the initial tool temperature distribution is the same for the same cutting conditions. The initial maximum temperature for 0.5, 1, and 1.5 mm depth of cut is 755 °C, 772 °C, and 895 °C, respectively. Therefore, the initial temperature distribution for the same cutting condition is only presented once, as shown in this subsection.

7.2.1 The effect of depth of cut for noncutting periods subjected to surrounding air

Figure 24 shows the temperature history for these three simulations with different depths of cut. The final temperature for 0.5, 1, and 1.5 mm depth of cut is 162 °C, 260 °C, and 342 °C, respectively. Figure 25 is a simplification of the temperature history only using the initial temperature and final temperature. It is manifest that the highest depth of cut has the highest initial temperature and highest final temperature and the depth of cut has great influence on final temperature distributions. It

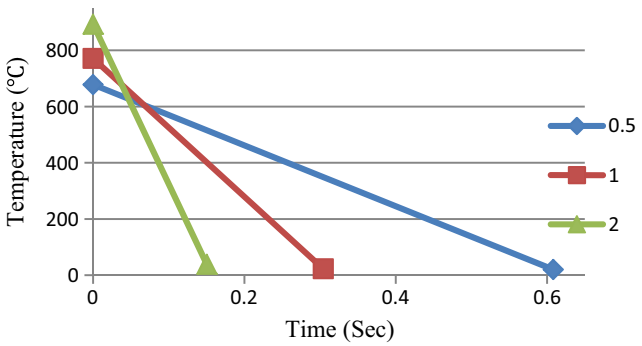

Fig. 17 Simplified temperature history for three different cutting speeds using only the initial and final temperatures for TrimSol 5 % concentrate water-based coolant

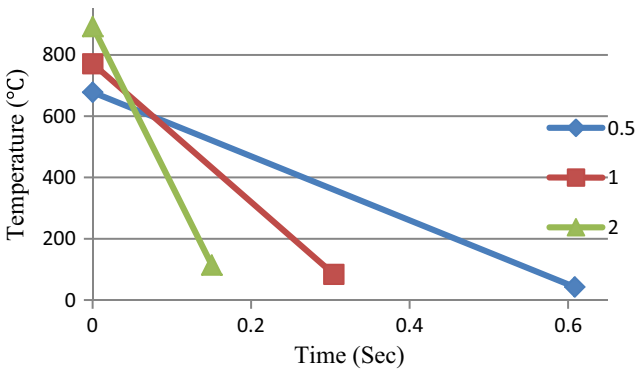

Fig. 19 Simplified temperature history for three different cutting speeds using only the initial and final temperatures for heavy duty water-soluble oil-based cutting fluid

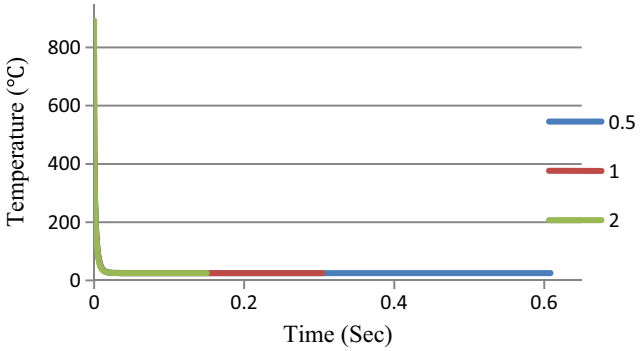

Fig. 20 Temperature history for three different cutting speeds for emulsion coolant

should be noted that for all of these three simulations, the final temperature distribution is uniform.

In Fig. 26a, the left plot shows the initial temperature distributions, and the right plot shows the internal horizontal segment cut out of the temperature distribution half way through for depth of cut 0.5 mm. In Fig. 26b, the left plot shows the initial temperature distributions, and the right plot shows the internal horizontal segment cut out of the temperature distribution half way through for depth of cut 1 mm. In Fig. 26c, the left plot shows the initial temperature distributions, and the right plot shows the internal horizontal segment cut out of the temperature distribution half way through for depth of cut 2 mm. It is noted that the lowest depth of cut has the lowest initial temperature distribution along the rake face and internally and the highest depth of cut has the highest initial temperature distribution along the rake face and internally. This helps to explain why depths of cut 0.5 and 1 mm can have almost the same initial temperature, but the final temperature for 1 mm depth of cut is higher than that of 0.5 mm depth of cut. It should be noted that in Fig. 26, all plots use the same legend scale so that there is no red zone in Fig. 26a because the red zone is for temperatures that are greater than 894 °C. The horizontal segment cut out in the right plot of 26a, 26b, and 26c starts at point 1 and continues to point 2.

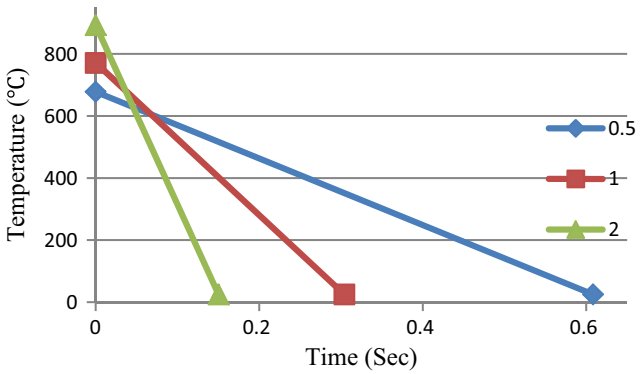

Fig. 21 Simplified temperature history for three different cutting speeds using only the initial and final temperatures for emulsion coolant

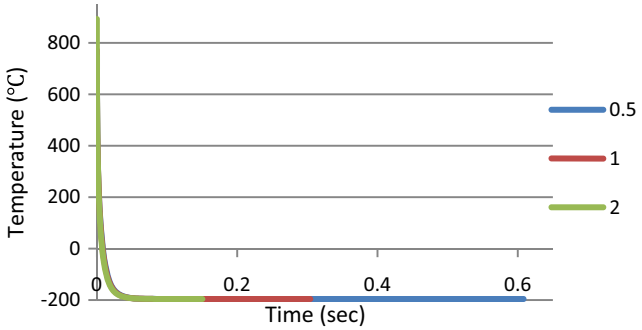

Fig. 22 Temperature history for three different cutting speeds for liquid nitrogen

7.2.2 The effect of depth of cut for noncutting periods subjected to TrimSol 5 % concentrate water-based coolant

Figure 27 shows the temperature history for these three simulations with different depths of cut. The final temperature for 0.5, 1, and 1.5 mm depth of cut is 22 °C, 23 °C, and 24 °C, respectively. Figure 28 is a simplification of the temperature history only using the initial temperature and final temperature. It is manifest that the highest depth of cut has the highest initial temperature and highest final temperature. It should be noted that for all of these three simulations, the final temperature distribution is uniform.

7.2.3 The effect of depth of cut for noncutting periods subjected to heavy duty water-soluble oil-based cutting fluid

Figure 29 shows the temperature history for these three simulations with different depths of cut. The final temperature for 0.5, 1, and 1.5 mm depth of cut is 58 °C, 85 °C, and 107 °C, respectively. Figure 30 is a simplification of the temperature history only using the initial temperature and final temperature. It is manifest that the highest depth of cut has the highest initial temperature and highest final temperature. It should be noted that for all of these three simulations, the final temperature distribution is uniform.

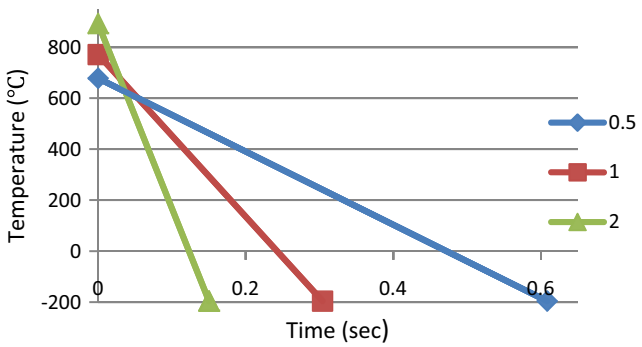

Fig. 23 Simplified temperature history for three different cutting speeds using only the initial and final temperatures for liquid nitrogen

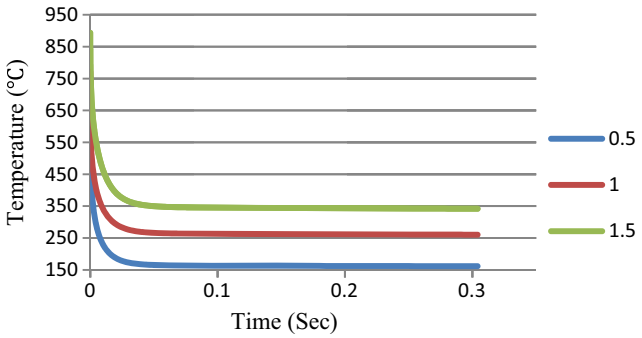

Fig. 24 Temperature history for the three depths of cut for surrounding air

7.2.4 The effect of depth of cut for noncutting periods subjected to emulsion coolant

Figure 31 shows the temperature history for these three simulations with different depths of cut. The final temperature for 0.5, 1, and 1.5 mm depth of cut is 25 °C, 25 °C, and 25 °C, respectively. Figure 32 is a simplification of the temperature history only using the initial temperature and final temperature. It is clearly seen that the highest depth of cut has the highest initial temperature and the lowest depth of cut has the lowest initial temperature with all of the cutting speeds having the same final temperature, the temperature of the coolant. It should be noted that for all of these three simulations, the final temperature distribution is uniform.

7.2.5 The effect of depth of cut for noncutting periods subjected to liquid nitrogen

Figure 33 shows the temperature history for these three simulations with different depths of cut. The final temperature for 0.5, 1, and 1.5 mm depth of cut is −196 °C, −196 °C, and −196 °C, respectively. Figure 34 is a simplification of the temperature history only using the initial temperature and final temperature. It is clearly seen that the highest depth of cut has the highest initial temperature and the lowest depth of cut has the lowest initial temperature with all of the cutting speeds having the same final temperature, the temperature of the coolant. It should be noted that for all of these three simulations, the final temperature distribution is uniform.

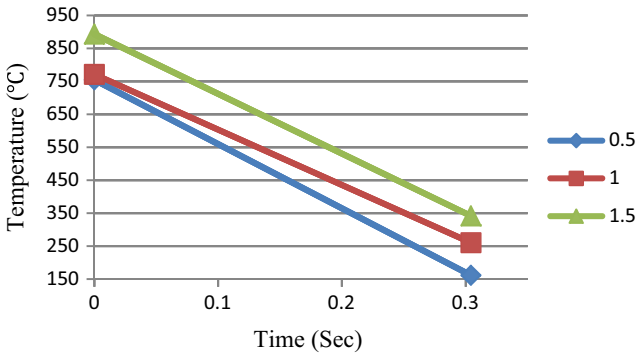

Fig. 25 Simplified temperature history for three depths of cut using only the initial and final temperatures for surrounding air

7.3 The effect of feed rate

In these simulations, feed rates (0.1, 0.2, and 0.4 mm/tooth). For all these simulations, the feed rate is 0.2 mm/tooth and axial depth of cut is 1 mm. The film coefficients (17.04, 5230, 1500, 87,500, and 3500 W/m^2 °C) and coolant temperatures (22.85, 20, 20, 25, and −196 °C) are changed, respectively (air, TrimSol 5 % concentrate water-based coolant, heavy duty water-soluble oil-based cutting fluid, emulsion coolant, and liquid nitrogen). It should be noted that for different coolants, the initial tool temperature distribution is the same for the same cutting conditions. Therefore, the initial temperature distribution for the same cutting condition is only presented once, as shown in this subsection. The initial temperatures for 0.1, 0.2, and 0.4 mm/tooth are 794, 772, and 850 °C, respectively.

7.3.1 The effect of feed rate for noncutting periods subjected to surrounding air

Figure 35 shows the temperature history for these three simulations. The final temperatures for 0.1, 0.2, and 0.4 mm/tooth are 254 °C, 260 °C, and 314 °C, respectively. Figure 36 is a simplification of the temperature history only using the initial temperature and final temperature. It is clearly seen that the highest feed rate has the highest initial temperature and highest final temperature. It is noted that for 0.1 and 0.2 mm/tooth, both the initial and final temperatures are very close. It can be concluded that the feed rate does not affect the initial and final temperatures very much when it changes from 0.1 to 0.2 mm/tooth. However, when the feed rate changes from 0.2 to 0.4 mm/tooth, it has significant influence on the initial and final temperatures. It should be noted that for all of these three simulations, the final temperature distribution is uniform.

In Fig. 37a, the left plot shows the initial temperature distributions, and the right plot shows the internal horizontal segment cut out of the temperature distribution half way through for feed rate 0.1 mm/tooth. In Fig. 37b, the left plot shows the initial temperature distributions, and the right plot shows the internal horizontal segment cut out of the temperature distribution half way through for feed rate 0.2 mm/tooth. In Fig. 37c, the left plot shows the initial temperature distributions, and the right plot shows the internal horizontal segment cut out of the temperature distribution half way through for feed rate 0.4 mm/tooth. It is noted that the lowest and middle feed rate have very close initial temperature distribution along the rake face and internally. The highest feed rate

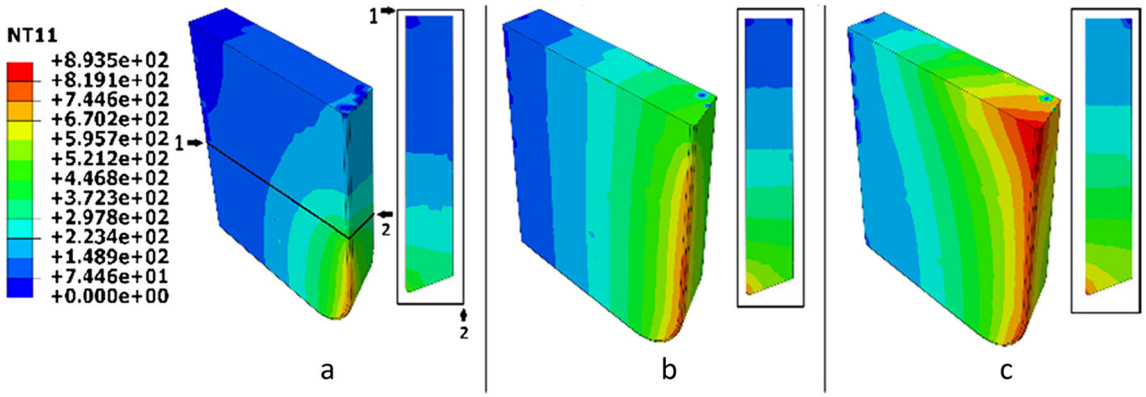

Fig. 26 Initial temperature distributions and internal horizontal segment cut out of the temperature distribution half way through for three different depths of cut (0.5, 1, and 2 mm respectively)

has the highest initial temperature distribution along the rake face and internally. This helps to explain why feed rates of 0.1 and 0.2 mm/tooth have very close final temperatures. It should be noted that in Fig. 37, all plots use the same legend scale so that there is no red zone in Fig. 37a, b because the red zone is for temperatures that are greater than 850 °C. The horizontal segment cut out in the right plot of 37a, 37b, and 37c starts at point 1 and continues to point 2.

7.3.2 The effect of feed rate for noncutting periods subjected to TrimSol 5 percent concentrate water-based coolant

Figure 38 shows the temperature history for these three simulations. The final temperatures for 0.1, 0.2, and 0.4 mm/tooth are 23 °C, 23 °C, and 24 °C, respectively. Figure 39 is a simplification of the temperature history only using the initial temperature and final temperature. It is clearly seen that the highest feed rate has the highest initial temperature and the lowest feed rate has the lowest initial temperature with all of the feed rates having close to the same final temperature. It should be noted that for all of these three simulations, the final temperature distribution is uniform.

7.3.3 The effect of feed rate for noncutting periods subjected to heavy duty water-soluble oil-based cutting fluid

Figure 40 shows the temperature history for these three simulations. The final temperatures for 0.1, 0.2, and 0.4 mm/tooth are 83 °C, 85 °C, and 98 °C, respectively. Figure 41 is a simplification of the temperature history only using the initial temperature and final temperature. It is clearly seen that the highest feed rate has the highest initial temperature and highest final temperature while the lowest feed rate has the lowest initial temperature and lowest final temperature. It should be noted that for all of these three simulations, the final temperature distribution is uniform.

7.3.4 The effect of feed rate for noncutting periods subjected to emulsion coolant

Figure 42 shows the temperature history for these three simulations. The final temperatures for 0.1, 0.2, and 0.4 mm/tooth are 25 °C, 25 °C, and 25 °C, respectively. Figure 43 is a simplification of the temperature history only using the initial temperature and final temperature. It is clearly seen that the

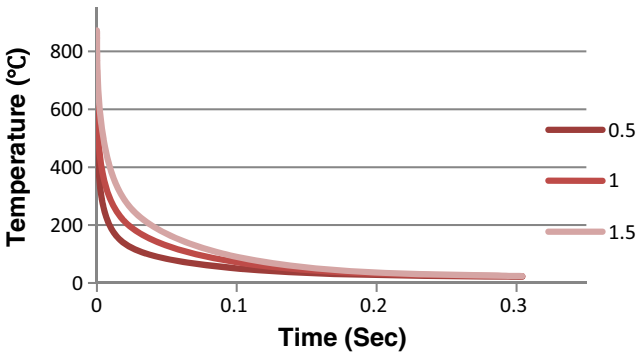

Fig. 27 Temperature histories for the three depths of cut for TrimSol 5 % concentrate water-based coolant

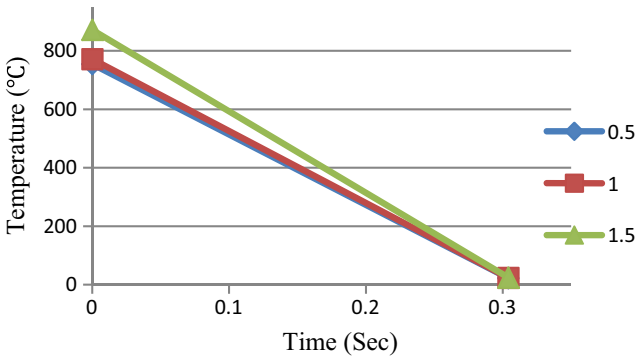

Fig. 28 Simplified temperature history for three depths of cut using only the initial and final temperatures for TrimSol 5 % concentrate water-based coolant

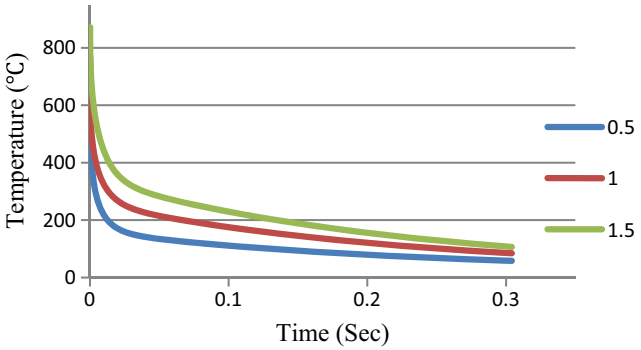

Fig. 29 Temperature history for the three depths of cut for heavy duty water-soluble oil-based cutting fluid

highest feed rate has the highest initial temperature and the lowest feed rate has the lowest initial temperature with all of the feed rates having the same final temperature, the temperature of the coolant. It should be noted that for all of these three simulations, the final temperature distribution is uniform.

7.3.5 The effect of feed rate for noncutting periods subjected to liquid nitrogen

Figure 44 shows the temperature history for these three simulations. The final temperatures for 0.1, 0.2, and 0.4 mm/tooth are −196, −196, −196 °C, respectively. Figure 45 is a simplification of the temperature history only using the initial temperature and final temperature. It is clearly seen that the highest feed rate has the highest initial temperature and the lowest feed rate has the lowest initial temperature with all of the feed rates having the same final temperature, the temperature of the coolant. It should be noted that for all of these three simulations, the final temperature distribution is uniform.

7.4 Comparison of the effect of cutting conditions for noncutting periods subjected to different coolants

To get the full understanding of how the coolants (surrounding air, TrimSol 5 % concentrate water-based coolant, heavy duty water-soluble oil-based cutting fluid, emulsion coolant, and liquid nitrogen) affect the tool temperature during the noncutting period; the temperature histories of each parameter are compared.

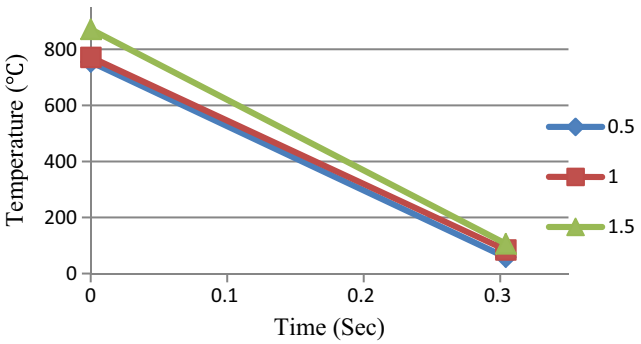

Fig. 30 Simplified temperature history for three depths of cut using only the initial and final temperatures for heavy duty water-soluble oil-based cutting fluid

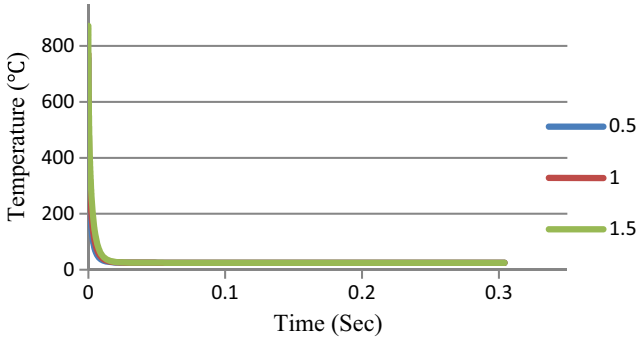

Fig. 31 Temperature history for the three depths of cut for emulsion coolant

7.4.1 Comparison of the effect of cutting speed/duration of time for noncutting periods subjected to different coolants

Figure 46 shows the temperature history of cutting speed 0.5 m/s subjected to the different coolants. It is clearly seen that subjected to air has the highest final temperature (323 °C), heavy duty water-soluble oil-based cutting fluid has then next highest final temperature (43 °C), TrimSol 5 % concentrate water-based coolant (flood) and emulsion coolant have the next coolest final temperature (20 and 25 °C, respectively) and liquid nitrogen has the lowest final temperature (−196 °C).

Figure 47 shows the temperature history of cutting speed 1 m/s subjected to the different coolants. It is clearly seen that subjected to air has the highest final temperature (260 °C), heavy duty water-soluble oil-based cutting fluid has then next highest final temperature (85 °C), TrimSol 5 % concentrate water-based coolant (flood), and emulsion coolant have the next coolest final temperature (23 and 25 °C, respectively), and liquid nitrogen has the lowest final temperature (−196 °C).

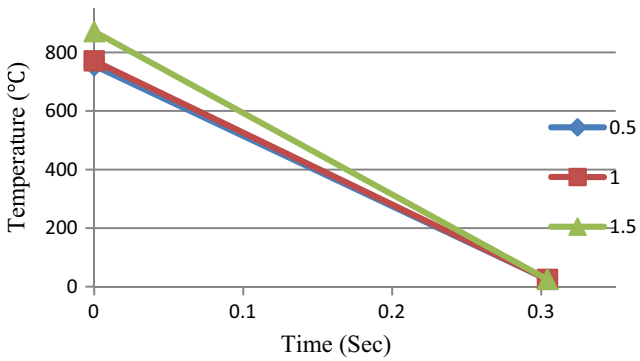

Fig. 32 Simplified temperature history for three depths of cut using only the initial and final temperatures for emulsion coolant

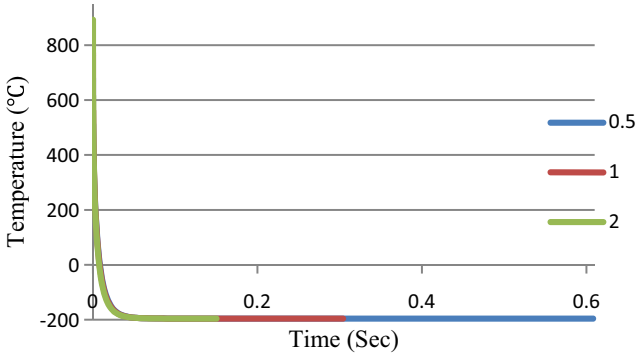

Fig. 33 Temperature history for the three depths of cut for liquid nitrogen

Figure 48 shows the temperature history of cutting speed 2 m/s subjected to the different coolants. It is clearly seen that subjected to air has the highest final temperature (203 °C), heavy duty water-soluble oil-based cutting fluid has then next highest final temperature (115 °C), TrimSol 5 % concentrate water-based coolant (flood) and emulsion coolant have the next coolest final temperature (39 and 25 °C, respectively) and liquid nitrogen has the lowest final temperature (−196 °C).

7.4.2 Comparison of the effect of depth of cut for noncutting periods subjected to different coolants

Figure 49 shows the temperature history of depth of cut 0.5 mm subjected to the different coolants. It is clearly seen that subjected to air has the highest final temperature (162 °C), heavy duty water-soluble oil-based cutting fluid has then next highest final temperature (58 °C), TrimSol 5 % concentrate water-based coolant (flood) and emulsion coolant have the next coolest final temperature (22 and 25 °C, respectively) and liquid nitrogen has the lowest final temperature (−196 °C).

Figure 50 shows the temperature history of depth of cut 1 mm subjected to the different coolants. It is clearly seen that subjected to air has the highest final temperature (260 °C), heavy duty water-soluble oil-based cutting fluid has then next highest final temperature (85 °C), TrimSol 5 % concentrate water-based coolant (flood) and emulsion coolant have the next coolest final temperature (39 and 25 °C, respectively) and liquid nitrogen has the lowest final temperature (−196 °C).

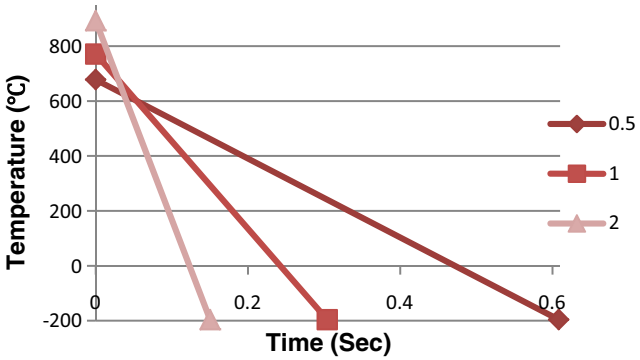

Fig. 34 Simplified temperature history for three depths of cut using only the initial and final temperatures for liquid nitrogen

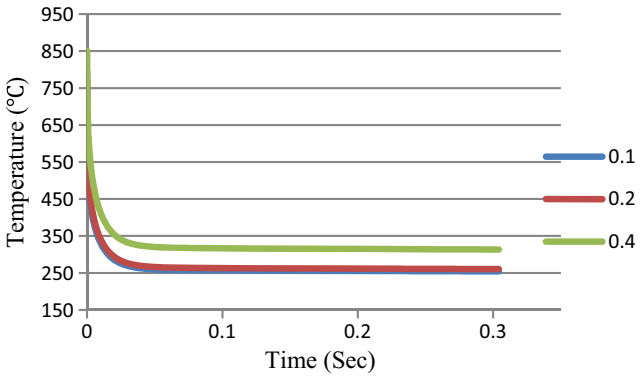

Fig. 35 Temperature history for three different feed rates for surrounding air

Figure 51 shows the temperature history of depth of cut 1.2 mm subjected to the different coolants. It is clearly seen that subjected to air has the highest final temperature (342 °C), heavy duty water-soluble oil-based cutting fluid has then next highest final temperature (107 °C), TrimSol 5 % concentrate water-based coolant (flood) and emulsion coolant have the next coolest final temperature (24 and 25 °C, respectively) and liquid nitrogen has the lowest final temperature (−196 °C).

7.4.3 Comparison of the effect of feed rate for noncutting periods subjected to different coolants

Figure 52 shows the temperature history of feed rate 0.1 mm/tooth subjected to the different coolants. It is clearly seen that subjected to air has the highest final temperature (254 °C), heavy duty water-soluble oil-based cutting fluid has then next highest final temperature (83 °C), TrimSol 5 % concentrate water-based coolant (flood) and emulsion coolant have the next coolest final temperature (23 and 25 °C, respectively) and liquid nitrogen has the lowest final temperature (−196 °C).

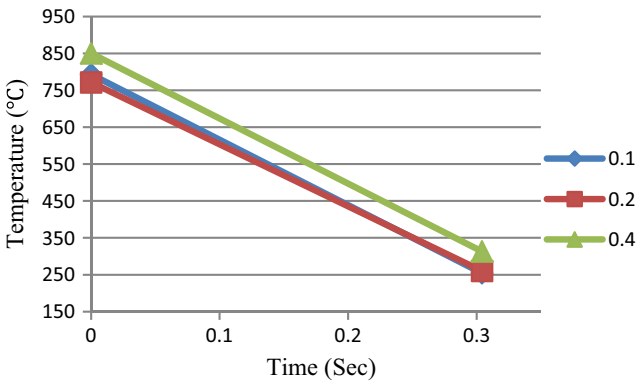

Fig. 36 Simplified temperature history for three different feed rates using only the initial and final temperatures for surrounding air

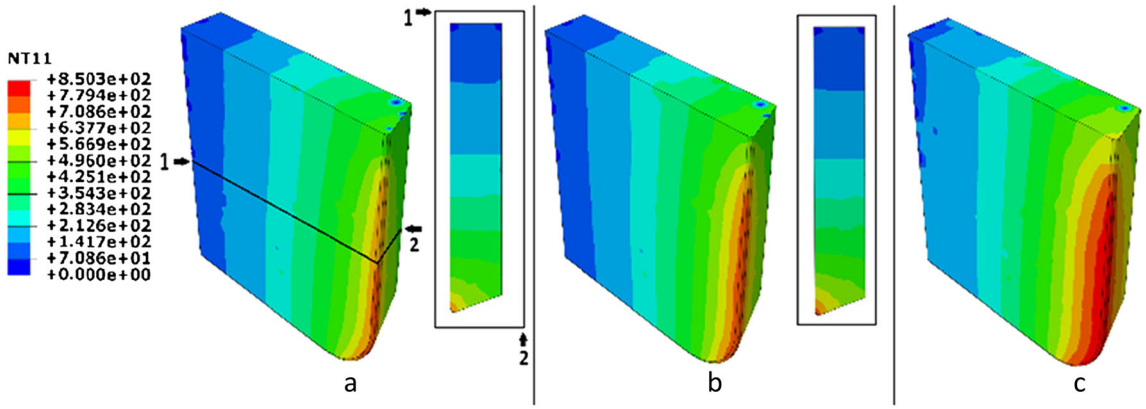

Fig. 37 Initial temperature distributions and internal horizontal segment cut out of the temperature distribution half way through for three different feed rates (0.1, 0.2, and 0.4 mm/tooth respectively)

Figure 53 shows the temperature history of feed rate 0.2 mm/tooth subjected to the different coolants. It is clearly seen that subjected to air has the highest final temperature (260 °C), heavy duty water-soluble oil-based cutting fluid has then next highest final temperature (85 °C), TrimSol 5 % concentrate water-based coolant (flood) and emulsion coolant have the next coolest final temperature (23 and 25 °C, respectively) and liquid nitrogen has the lowest final temperature (−196 °C).

Figure 54 shows the temperature history of feed rate 0.4 mm/tooth subjected to the different coolants. It is clearly seen that subjected to air has the highest final temperature (314 °C), heavy duty water-soluble oil-based cutting fluid has then next highest final temperature (98 °C), TrimSol 5 % concentrate water-based coolant (flood) and emulsion coolant have the next coolest final temperature (24 and 25 °C, respectively) and liquid nitrogen has the lowest final temperature (−196 °C).

Knowing all of the trends of the temperature history of all simulations seen in Figs. 46, 47, 48, 49, 50, 51, 52, 53, and 54, it can be seen that liquid nitrogen is most effective in reducing the temperature of the tool due to the fact that it consistently cools the tool in the least amount of time, emulsion coolant is the second most efficient coolant used, TrimSol 5 % concentrate water-based coolant (flood) is the third most efficient coolant, heavy duty water-soluble oil-based cutting fluid is the fourth most efficient coolant, and surrounding air is least efficient coolant scheme used.

7.4.4 Comparison of the effect of different coolants on the final temperature for noncutting periods

Due to the low thermal conductivity of Ti alloys, which is an inherent property of this group of materials, it is highly desirable that the temperature of tool insert can be lowered to room temperature after tool insert disengages the workpiece in order to avoid the accumulation of the heat along tool-chip contact length when the tool insert engages the workpiece again. The aim of this research is to investigate the effects of different cooling schemes during the noncutting period of the milling process to lower the temperature of the tool insert before the tool insert reengages the workpiece. This research provides insights of cutting conditions and cooling schemes under which tool life can be increased.

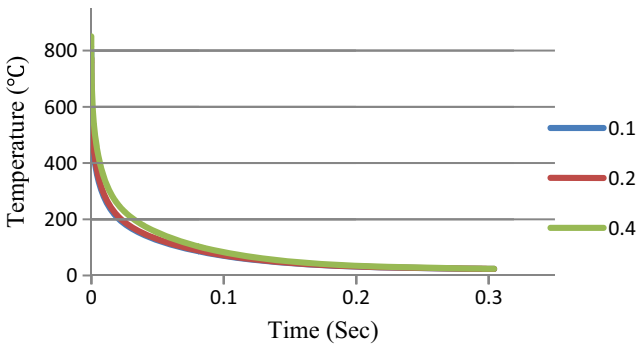

Fig. 38 Temperature histories for three different feed rates for TrimSol 5 % concentrate water-based coolant

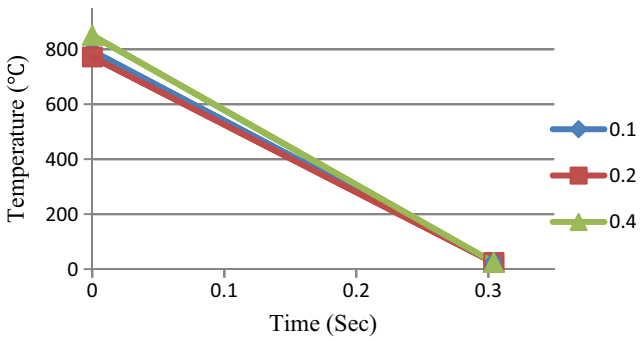

Fig. 39 Simplified temperature histories for three different feed rates using only the initial and final temperatures for TrimSol 5 % concentrate water-based coolant

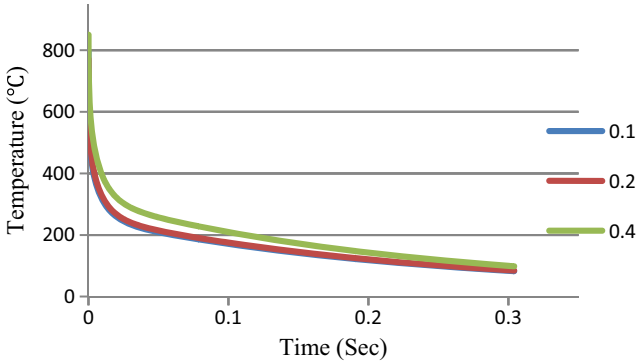

Fig. 40 Temperature histories for three different feed rates for heavy duty water-soluble oil-based cutting fluid

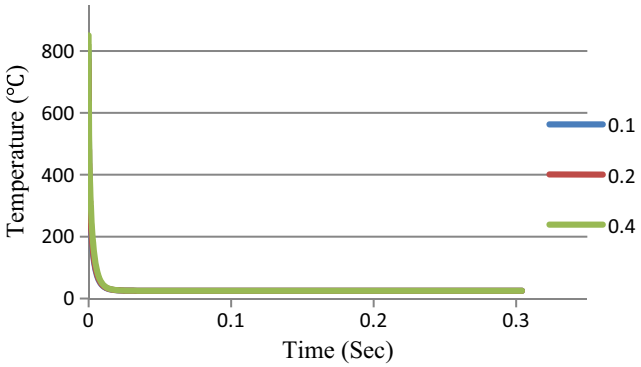

Fig. 42 Temperature history for three different feed rates for emulsion coolant

Figure 55 shows the comparison of the final temperatures for the three cutting speeds (0.5, 1, 2 m/s). It is clearly seen that surrounding air has the highest final temperatures, and as the cutting speeds increase, the final temperatures decrease (323, 260 °C, 203°, respectively). Heavy duty water-soluble oil-based cutting fluid has the next highest final temperature with the cutting speed of 0.5 mm being closest to room temperature and the other final temperatures increasing as the cutting speed increases (43, 85, 115 °C, respectively). TrimSol 5 % concentrate water-based coolant (flood) consistently reduces the final temperatures of the insert close to room temperature with little variation between each final temperature but as the cutting speed increases so does the final temperature (20, 23 °C, 39°). Emulsion coolant consistently reduces the final temperatures of the insert close to room temperature with no variation of the coolant and equaling the temperature of the coolant (25 °C). Liquid nitrogen has the lowest final temperatures with the temperatures being the same and equaling the temperature of the coolant (−196 °C). Based on Fig. 55, it is manifested that for different coolants, the final temperature of tool may change differently as the cutting speed changes. This can be explained as follows: During the cooling process, the final temperature of the tool is affected by three factors: cooling time, film coefficient of the coolant, and the initial amount of heat in the tool before cooling process begins. When the film coefficient is low (for the air, of which the film coefficient is 17.04 W/m^2 °C), the final temperature is mainly determined by the initial amount of heat in the tool since the heat transfer rate is very small. When the cutting speed is high, the initial surface temperature of the tool obtained when the milling process ends is higher than that of lower cutting speed. However, the initial amount of heat for higher cutting speed is lower than that of lower cutting speed. Consequently, when air is used as the coolant, the final temperature (the final amount of heat) for higher cutting speed is lower. When the film coefficient is high (for flood, heavy duty water-soluble oil-based cutting fluid, of which the film coefficients are 1500 and 5230 W/m^2 °C, respectively), the final temperature is mainly determined by the amount of heat transferred during cooling process, which is the product of the film coefficient and the cooling time. Because the cooling time for higher cutting speed is smaller than that for lower cutting speed, the amount of heat transferred for higher cutting speed is smaller. Consequently, the final amount of heat (final temperature) will be higher for high cutting speed. When the film coefficient is extremely high (for emulsion coolant and liquid nitrogen, of which the film coefficients are 87,500 and

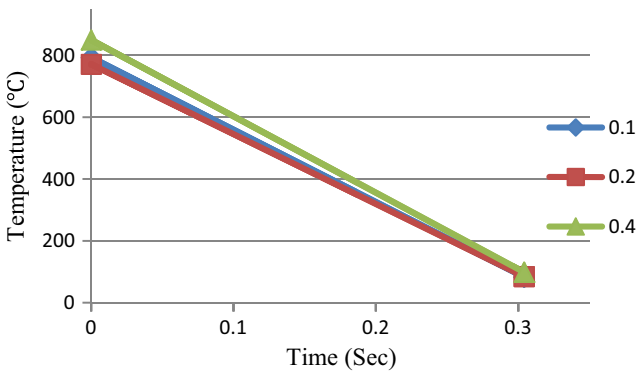

Fig. 41 Simplified temperature histories for three different feed rates using only the initial and final temperatures for heavy duty water-soluble oil-based cutting fluid

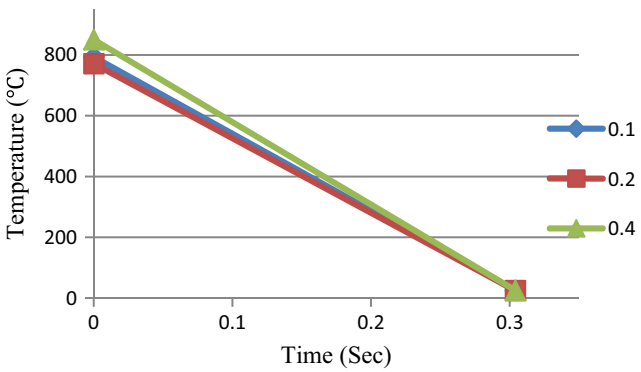

Fig. 43 Simplified temperature histories for three different feed rates using only the initial and final temperatures for emulsion coolant

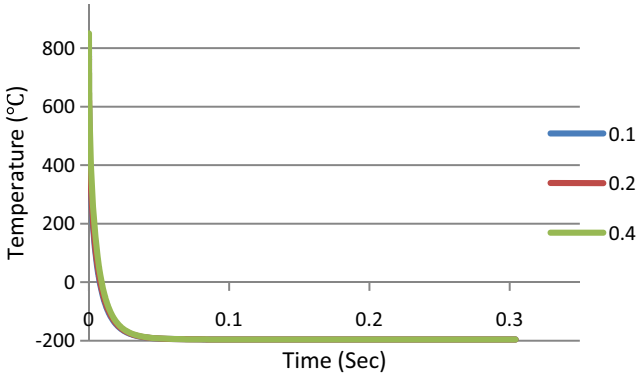

Fig. 44 Temperature history for three different feed rates for liquid nitrogen

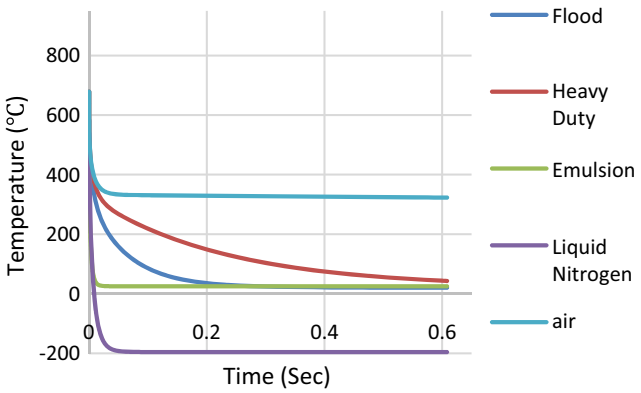

Fig. 46 Temperature history for cutting speed of 0.5 m/s subjected to coolants

35,000 W/m^2 °C, respectively), the final amount of heat (final temperature) will be the same for all cutting speeds.

Figure 56 shows the comparison of the final temperatures for the three depths of cut (0.5, 1, 1.5 mm). It is clearly seen that surrounding air has the highest final temperature and as the depth of cut increases so does the final temperatures (162, 260, 342 °C, respectively). Heavy duty water-soluble oil-based cutting fluid has the next highest final temperature with the depth of cut of 0.5 mm being closest to room temperature and the other final temperatures increasing as the depth of cut increases (58, 85, 107 °C, respectively). TrimSol 5 % concentrate water-based coolant (flood) is able to reduce the final tool temperature close to room temperature and is almost the exact same temperature for all the depths of cut (22, 23, 24 °C, respectively). Emulsion coolant consistently reduces the final temperatures of the insert near the room temperature which is also the temperature of the coolant (25 °C). Liquid nitrogen has the lowest final temperatures with the temperatures being the same and equaling the temperature of the coolant (−196 °C).

Figure 57 shows the comparison of the final temperatures for the three feed rates (0.1, 0.2, 0.4 mm/tooth). It is clearly seen that surrounding air has the highest final temperature and as the feed rate increases so does the final temperatures (254, 260, 314 °C, respectively). Heavy duty water-soluble oil-based cutting fluid has the next highest final temperature with little change in the final temperature as the feed rate increases (83, 85, 98 °C, respectively). TrimSol 5 % concentrate water-based coolant (flood) is able to reduce the final tool temperature close to room temperature and is almost the exact same temperature for all the feed rates (23, 23, 24 °C, respectively). Emulsion coolant consistently reduces the final temperatures of the insert near the room temperature which is also the temperature of the coolant (25 °C). Liquid nitrogen has the lowest final temperatures with the temperatures being the same and equaling the temperature of the coolant (−196 °C).

7.5 The effects of cutting conditions with cooling schemes during the noncutting periods on thermal stress

Due to the cyclic loading nature of milling processes, heating during cutting stage and cooling during noncutting stage cause cyclic, thermal stress in tool insert. In this section, the thermal stress is investigated using the change in temperature of the hottest point on the insert for the simulations. This provides insights of the possibility of thermal cracking due to the cyclic thermal stress.

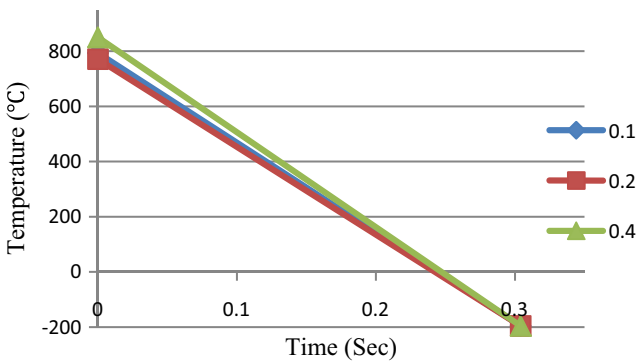

Fig. 45 Simplified temperature histories for three different feed rates using only the initial and final temperatures for liquid nitrogen

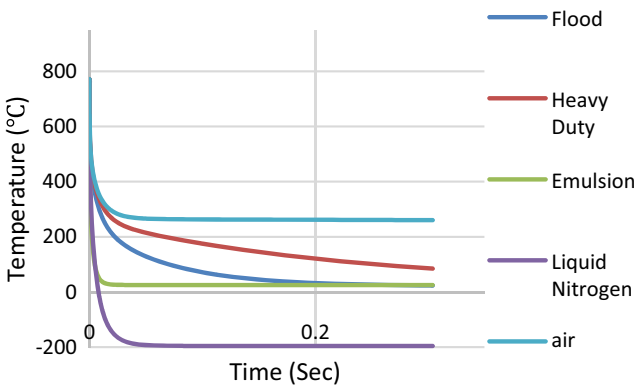

Fig. 47 Temperature history for cutting speed of 1 m/s subjected to coolants

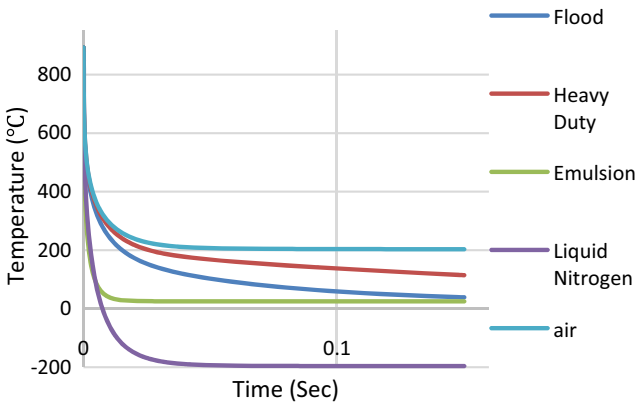

Fig. 48 Temperature history for cutting speed of 2 m/s subjected to coolants

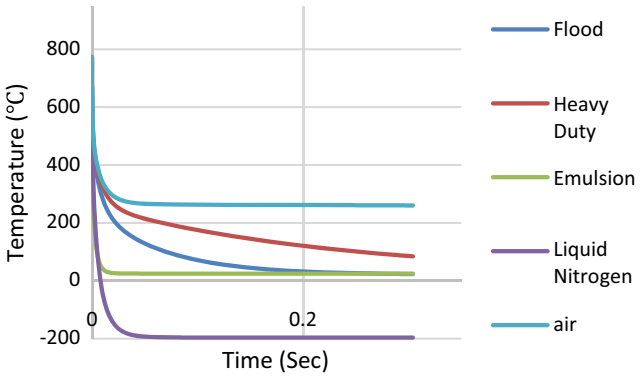

Fig. 50 Temperature history for depth of cut of 1 mm subjected to coolants

7.5.1 The effects of cutting speeds with cooling schemes during the noncutting periods on thermal stress

Figure 58 shows that the thermal stress of the three cutting speeds (0.5, 1, 2 m/s) subjected to the different coolants. The thermal stress for the three simulations varying the cutting speed subjected to the surrounding air is 1.78, 2.56, 3.45 GPa, respectively. It is clearly seen for the simulations subjected to the surrounding air that the highest cutting speed has the highest thermal stress and the lowest cutting speed has the lowest thermal stress. The thermal stress for the three simulations varying the cutting speed subjected to 5 % concentrate water-based coolant is 3.29, 3.75, 4.28 GPa, respectively. It is clearly seen for the simulations subjected to 5 % concentrate water-based coolant that the highest cutting speed has the highest thermal stress and the lowest cutting speed has the lowest thermal stress. The thermal stress for the three simulations varying the cutting speed subjected to heavy duty water-soluble oil-based cutting fluid is 3.18, 3.44, 3.90 GPa, respectively. It is clearly seen for the simulations subjected to heavy duty water-soluble oil-based cutting fluid that the highest cutting speed has the highest thermal stress and the lowest cutting speed has the lowest thermal stress. The thermal stress for the three simulations varying the cutting speed subjected to emulsion coolant is 3.27, 3.74, 4.34 GPa, respectively. It is clearly seen that the highest cutting speed has the highest thermal stress and the lowest cutting speed has the lowest thermal stress. The thermal stress for the three simulations varying the cutting speed subjected to liquid nitrogen is 4.37, 4.85, 5.45 GPa, respectively. It is clearly seen for the simulations subjected to liquid nitrogen that the highest cutting speed has the highest thermal stress and the lowest cutting speed has the lowest thermal stress.

By comparing the thermal stress of the different coolants, it is clearly seen that the simulations subject to air have the lowest thermal stress and the simulations subjected to liquid nitrogen have the highest thermal stress.

7.5.2 The effects of depths of cut with cooling schemes during the noncutting periods on thermal stress

Figure 59 shows that the thermal stress of the three depths of cut (0.5, 1, 1.5 mm) subjected to the different coolants. It shows that the thermal stress for the three simulations varying the depths subjected to the surrounding air is 2.95, 2.56,

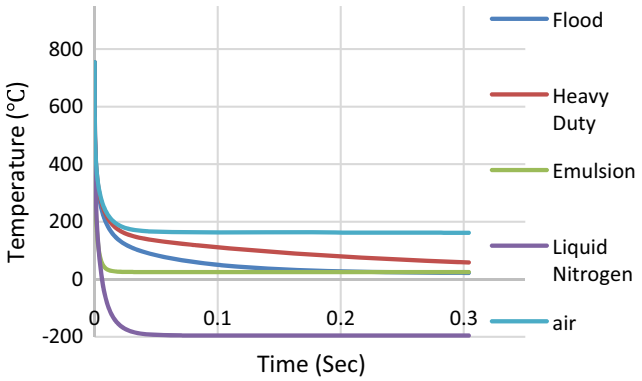

Fig. 49 Temperature history for depth of cut of 0.5 mm subjected to coolants

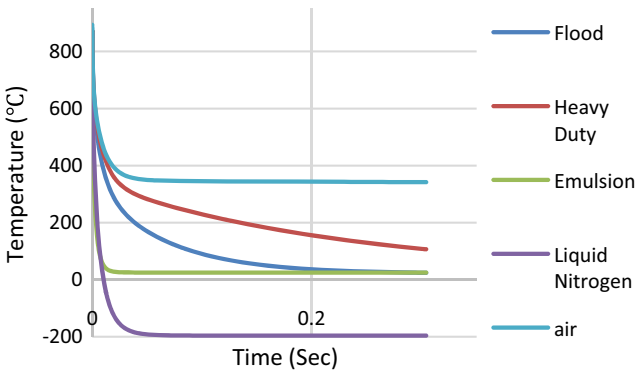

Fig. 51 Temperature history for depth of cut of 1.5 mm subjected to coolants

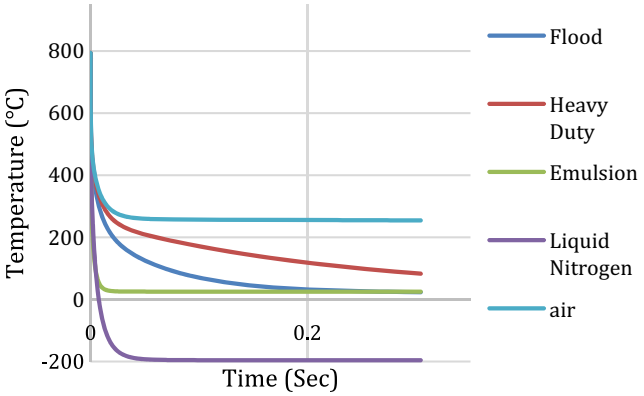

Fig. 52 Temperature history for feed rate of 0.1 mm/tooth subjected to coolants

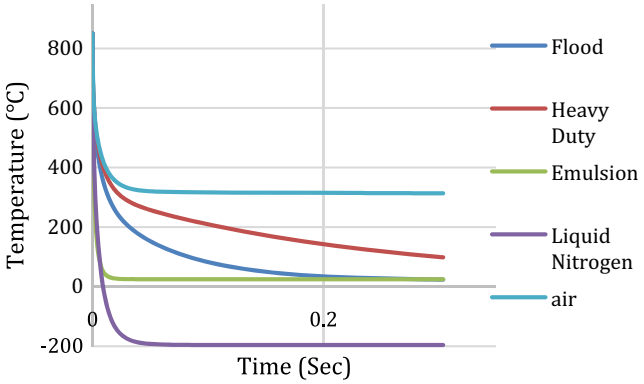

Fig. 54 Temperature history for feed rate of 0.4 mm/tooth subjected to coolants

2.77 GPa, respectively. It is clearly seen for the simulations subjected to surrounding air that the middle depth of cut, 1 mm, has the lowest thermal stress. The thermal stress for the three simulations varying the depths of cut subjected to TrimSol 5 % concentrate water-based coolant is 3.67, 3.75, 4.36 GPa, respectively. It is clearly seen that for the simulations subjected to TrimSol 5 % concentrate water-based coolant the lowest depth of cut has the lowest thermal stress and the highest depth of cut has the highest thermal stress. The thermal stress for the three simulations varying the depths of cut subjected to heavy duty water-soluble oil-based cutting fluid is 3.49, 3.44, 3.95 GPa, respectively. It is clearly seen for the simulations subjected to heavy duty water-soluble oil-based cutting fluid that the middle depth of cut, 1 mm, has the lowest thermal stress. The thermal stress for the three simulations varying the depths of cut subjected to emulsion coolant is 3.65, 3.74, 4.35 GPa, respectively. It is clearly seen for the simulations subjected to emulsion coolant that the highest depth of cut has the highest thermal stress and the lowest depth of cut has the lowest thermal stress. The thermal stress for the three simulations varying the depths of cut subjected to liquid nitrogen is 4.76, 4.85, 5.46 GPa, respectively. It is clearly seen for the simulations subjected to liquid nitrogen that the highest depth of cut has the highest thermal stress and the lowest depth of cut has the lowest thermal stress.

It is clearly seen that the simulations subjected to air have the lowest thermal stress and the simulations subjected to liquid nitrogen have the highest thermal stress.

7.5.3 The effects of feed rates with cooling schemes during the noncutting periods on thermal stress

Figure 60 shows that the thermal stress of the three feed rates (0.1, 0.2, 0.4 mm/tooth) subjected to the different coolants. It is clearly seen that the simulations subjected to air have the lowest thermal stress and the simulations subjected to liquid nitrogen have the highest thermal stress.

Figure 60 shows the thermal stress for the three simulations varying the feed rates subjected to the surrounding air is 2.70, 2.56, 2.69 GPa, respectively. It is clearly seen the simulations subjected to surrounding air that the middle feed rate, 0.2 mm/tooth, has the lowest thermal stress. The thermal stress for the three simulations varying the feed rates subjected to the TrimSol 5 % concentrate water-based coolant is 3.86, 3.75, 4.14 GPa, respectively. It is clearly seen the simulations subjected to TrimSol 5 % concentrate water-based coolant that the

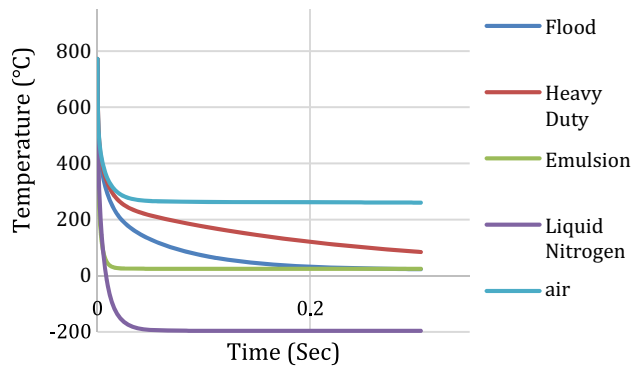

Fig. 53 Temperature history for feed rate of 0.2 mm/tooth subjected to coolants

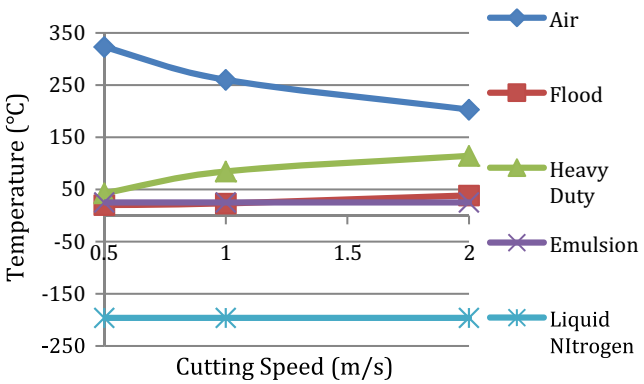

Fig. 55 Comparison of final temperatures for cutting speeds subjected to different coolants

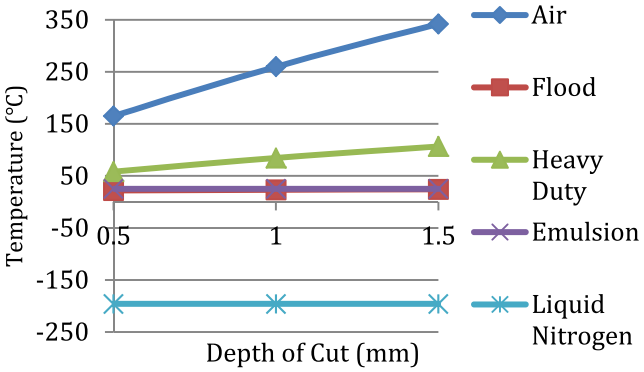

Fig. 56 Comparison of final temperatures for depths of cut subjected to different coolants

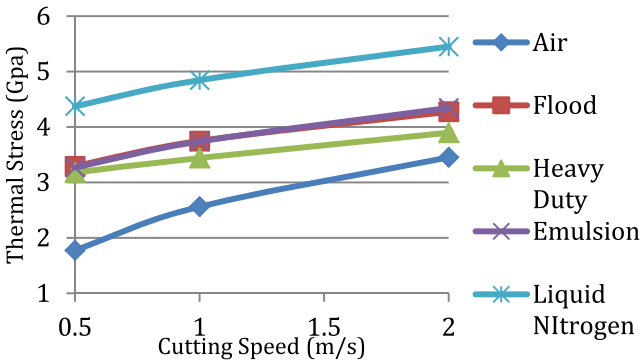

Fig. 58 Comparison of thermal stress for three different cutting speeds subjected to different coolants

middle feed rate has the lowest thermal stress. The thermal stress for the three simulations varying the feed rates subjected to heavy duty water-soluble oil-based cutting fluid is 3.56, 3.44, 3.76 GPa, respectively. It is clearly seen the simulations subjected to heavy duty water-soluble oil-based cutting fluid that the middle feed rate, 0.2 mm/tooth, has the lowest thermal stress. The thermal stress for the three simulations varying the feed rates subjected to emulsion coolant is 3.85, 3.74, 4.13 GPa, respectively. It is clearly seen the simulations subjected to emulsion coolant that the middle feed rate, 0.2 mm/tooth, has the lowest thermal stress. The thermal stress for the three simulations varying the feed rates subjected to liquid nitrogen. The thermal stress for 0.1, 0.2, and 0.4 mm/tooth is 4.96, 4.85, 5.24 GPa, respectively. It is clearly seen the simulations subjected to liquid nitrogen that the middle feed rate, 0.2 mm/tooth, has the lowest thermal stress.

8 Conclusions

In this paper, AdvantEdge FEM is used to model and simulate three dimensional (3D) corner up milling of Ti-6Al-4V to investigate the effects of cutting conditions (cutting speed, feed rate, and axial depth of cut) on temperature of the tool rake face and use Abaqus to conduct heat transfer analysis after the tool disengages the workpiece while being subjected to different cooling schemes before it reengages the workpiece. The tool material used is general carbide, and Johnson-Cook plastic model is utilized to model behavior of the workpiece Ti-6Al-4V. The 4-node linear heat transfer tetrahedron elements (DC3D4) are used in Abaqus heat transfer model. The convergence tests are conducted, and sensitivity test of the film coefficient is carried out.

New findings are the following:

1. For all sets of cutting conditions along with various cooling schemes, the final tool temperature is uniform throughout the tool insert.
2. Cutting speed has a large influence on the tool temperature distribution. The higher cutting speed generates higher initial temperature distribution along the rake face and lower internal temperature in the tool. When subjected to the surrounding air, final tool temperature decreases as the cutting speed increases. When subjected to the TrimSol 5 % concentrate water-based coolant and heavy duty water-soluble oil-based cutting fluid, final tool temperature increases as the cutting speed increases. When

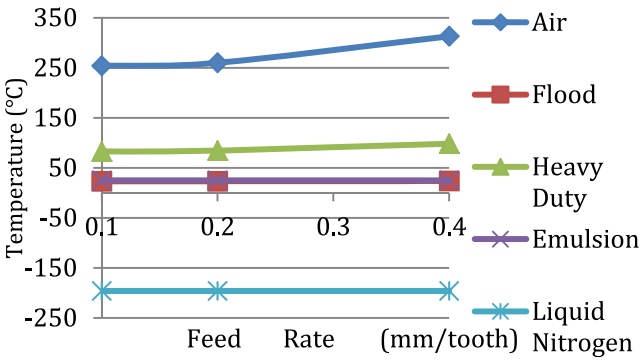

Fig. 57 Comparison of final temperatures for feed rates subjected to different coolants

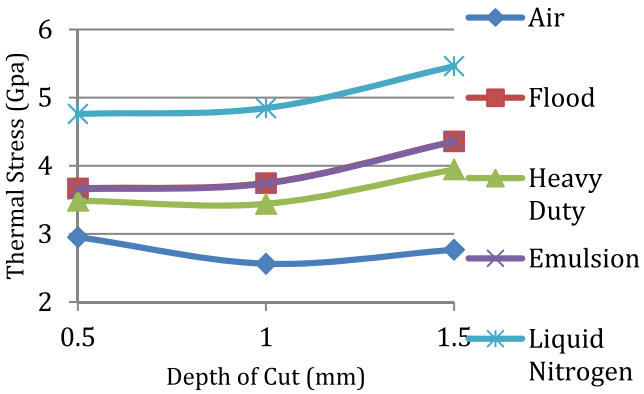

Fig. 59 Comparison of thermal stress for three different depths of cut subjected to different coolants

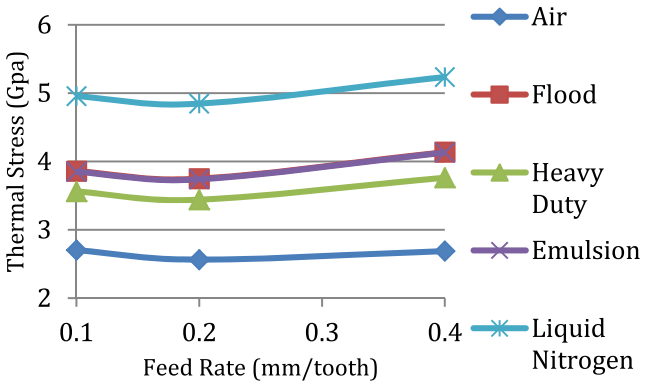

Fig. 60 Comparison of thermal stress for three different feed rates subjected to different coolants

subjected to the emulsion coolant and liquid nitrogen, the final tool temperature equals the temperature of the coolant for all different cutting speeds. The cooling scheme that consistently reduces the final tool temperature for the cutting speeds to room temperature or near; therefore, the possible optimal cooling scheme is the emulsion coolant and TrimSol 5 % concentrate water-based coolant. For all cutting speed simulations, no matter what coolant the insert is subjected to, as the cutting speed increases the higher the thermal stress.

3. Axial depth of cut also has a large influence on the tool temperature distribution. When subjected to all cooling schemes, the higher depth of cut gives the higher initial tool temperature. However, the initial temperature between depth of cut of 0.5 and 1 mm is not proportional to the change of the depth of cut. This results in a lower change in temperature during the cooling period and consequently reduces thermal stress when 1 mm depth of cut is used. This gives us the guidance that 1 mm depth of cut might be the optimal value to control the tool temperature while still maintaining an acceptable material removal rate (MRR). When subjected to the surrounding air, TrimSol 5 % concentrate water-based coolant, and heavy duty water-soluble oil-based cutting fluid; as the depth of cut increases so does the finial temperature which is almost proportional to the change of the depth of cut. When subjected to the emulsion coolant and liquid nitrogen, the final temperature equals the temperature of the coolant no matter the change in depth of cut. The cooling scheme that consistently reduces the final tool temperature for the cutting speeds to room temperature or near, there for the possible optimal cooling scheme, is the emulsion coolant and TrimSol 5 % concentrate water-based coolant. For simulations subjected to TrimSol 5 % concentrate water-based coolant and emulsion coolant, simulations with increased depths of cut had a higher thermal stress but the depths of cuts of 0.5 and 1 mm have little change in thermal stress. For simulations subjected to surrounding air, heavy duty water-soluble oil-based cutting fluid, and liquid nitrogen, the depth of cut of 1 mm has the lowest thermal stress. Thus, giving us more guidance that 1 mm depth of cut might be the optimal value to maintain an acceptable material removal rate (MRR) and results in lowest thermal stress.
4. Feed rate has large influence on the tool peak temperatures. When subjected to the surrounding air, TrimSol 5 % concentrate water-based coolant, heavy duty water-soluble oil-based cutting fluid, emulsion coolant, and liquid nitrogen; the feed rate does not affect the initial temperature very much when it changes from 0.1 to 0.2 mm/tooth. However, when the feed rate changes from 0.2 to 0.4 mm/tooth, it has significant influence on the initial temperature. Also, when subjected to the surrounding air, TrimSol 5 % concentrate water-based coolant, and heavy duty water-soluble oil-based cutting fluid; the feed rate does not affect the final temperature very much when it changes from 0.1 to 0.2 mm/tooth. However, when the feed rate changes from 0.2 to 0.4 mm/tooth, it has significant influence on the final temperature. This gives us guidance that 0.2 mm feed rate might be an optimal value to control the tool temperature while still maintaining an acceptable material removal rate (MRR). When subjected to the emulsion coolant and liquid nitrogen, the final temperature equals the temperature of the coolant no matter the change in depth of cut. The cooling scheme that consistently reduces the final tool temperature for the cutting speeds to room temperature or near, there for the possible optimal cooling scheme, is the emulsion coolant and TrimSol 5 % concentrate water-based coolant. For all feed rate simulations, no matter what coolant the insert is subjected to, the feed rate of 0.2 mm/tooth has the lowest thermal stress. Thus, giving us more guidance that 0.2 feed rate might be the optimal value to control the tool temperature while still maintaining an acceptable material removal rate (MRR)

References

1. Bermingham M, Kirsch J, Sun S, Palanisamy S, Dargusch M (2011) New observations on tool life, cutting forces and chip morphology in cryogenic machining Ti-6Al-4V. Int J Mach Tools Manuf 51:500–511
2. Liu P, Xu J, Fu Y (2011) Cutting force and its frequency spectrum characteristics in high speed milling of titanium alloy with a polycrystalline diamond tool. J Zhejiang Univ (Sci) 12(1):56–62
3. Oosthuizen GA, Akdogan G, Treurnicht N (2011) The performance of PCD tools in high-speed milling of Ti6Al4V. Int J Adv Manuf Technol 52(9–12):929–935
4. Ghani MU, Abukhshim NA, Sheikh MA (2008) An investigation of heat partition and tool wear in hard turning of h13 tool steel with cbn cutting tools. Int J Adv Manuf Technol 39(9–10):874–888

5. Alam S, Amin AN (2011) Surface roughness prediction in high speed flat end milling of Ti-Al6-V4 and optimization by desirability function of RSM. Adv Mater Res 264–265:1166–1173
6. Li L, Chang H, Wang M, Zuo DW, He L (2004) Temperature measurement in high speed milling Ti-Al6-V4. Key Eng Mater 259–260:804–808
7. Yang K, Liang Y, Zheng K, Bai Q, Chen W (2011) Tool edge radius effect on cutting temperature in micro-end-milling process. Int J Adv Manuf Technol 52(9–12):905–912
8. Rao B, Dandekar CR, Shin YC (2011) An experimental and numerical study on the face milling of Ti–6Al–4V alloy: tool performance and surface integrity. J Mater Process Technol 211(2):294–304
9. Yang Y, Li JF (2010) Study on mechanism of chip formation during high-speed milling of alloy cast iron. Int J Adv Manuf Technol 46(1–4):43–50
10. Li R, Hegde P, Shih AJ (2007) High-throughput drilling of titanium alloys. Int J Mach Tools Manuf 47(1):63–74
11. Li R, Riester L, Watkins TR, Blau PJ, Shih AJ (2008) Metallurgical analysis and nanoindentation characterization of Ti–6Al–4V workpiece and chips in high-throughput drilling. Mater Sci Eng A 472(1–2):115–124
12. Li R, Shih AJ (2006) Finite element modeling of 3D turning of titanium. Int J Adv Manuf Technol 29(3–4):253–261
13. Wang ZG, Rahman M, Wong YS, Sun J (2005, May) Modeling of cutting forces during machining of ti-al6-v4 with different coolant strategies. 8th CIRP International Workshop on Modeling in Machining Operations, Chemnitz, Germany
14. Huang X, Yao C (2011) Simulation of the high-speed machining temperature of titanium alloy. Adv Mater Res 314–316:1171–1175
15. Soo SL, Dewes RC, Aspinwall DK (2010) 3D FE modelling of high-speed ball nose end milling. Int J Adv Manuf Technol 50(9–12):871–882
16. Saffar RJ, Razfar M, Zarei O, Ghassemieh E (2008) Simulation of three-dimension cutting force and tool deflection in the end milling operation based on finite element method. Simul Model Pract Theory 16(10):1677–1688
17. Ali MH, Khidhir BA, Ansari M, Mohamed B (2013) FEM to predict the effect of feed rate on surface roughness with cutting force during face milling of titanium alloy. HBRC J 9(3):263–269
18. Wu H, Mayer J (1979) An analysis of thermal cracking of carbide tools in intermittent cutting. J Manuf Sci Eng 101(2):159–144
19. Chakraverti G, Pandey P, Mehta N (1984) Analysis of tool temperature fluctuation in interrupted cutting. Precis Eng 6(2):99–105
20. AdvantEdge FEM (2013) User's manual, version 6.1
21. Dandekar C, Shin Y, Barbes J (2010) Machinability improvement of Ti-6Al-4V via LAM and hybrid machining. Int J Mach Tools Manuf 50(2):174–182
22. Granta's CES EduPack (2007) Granta material intelligence. Granta design limited
23. Mills KC (2002) Recommended values of thermophysical properties for selected commercial alloys. Woodhead, Cambridge
24. Abaqus FEM (2012) User's manual, version 6.12
25. Mamalis A, Horváth M, Branis A, Manolakos D (2001) Finite element simulation of chip formation in orthogonal metal cutting. J Mater Process Technol 110(1):19–27
26. Kurgin S, Dasch J, Simon D, Barber G, Zou Q (2012) Evaluation of the convective heat transfer coefficient for minimum quantity lubrication (MQL). Ind Lubr Tribol 64(6):376–86
27. Cheng Y, Liu L, Sun S, Qian J, Gong Y, Wu M (2013) Influence of thermal load on mechanical property of cemented carbide material and heavy cemented carbide inserts life. J Harbin Inst Technol 20(6):59–66
28. Chakraverti G, Pandey P, Mehta N (1984) Analysis of tool temperature fluctuation in interrupted cutting. Precis Eng 6(2):99–105
29. Li A, Zhao J, Luo H, Pei Z, Wang Z (2012) Progressive tool failure in high-speed dry milling of Ti-6Al-4V alloy with coated carbide tools. Int J Adv Manuf Technol 58(5–8):465–478